Ultra-Wideband Communications

An Idea Whose Time Has Come

Ultra-wideband (UWB) radio is a fast emerging technology with uniquely attractive features inviting major advances in wireless communications, networking, radar, imaging, and positioning systems. By its rule-making proposal in 2002, the Federal Communications Commission (FCC) in the United States essentially unleashed huge "new bandwidth" (3.6–10.1 GHz) at the noise floor, where UWB radios overlaying coexistent RF systems can operate using low-power ultra-short information bearing pulses. With similar regulatory processes currently under way in many countries worldwide, industry, government agencies, and academic institutions responded to this FCC ruling with rapidly growing research efforts targeting a host of exciting UWB applications: short-range very high-speed broadband access to the Internet, covert communication links, localization at centimeter-level accuracy, high-resolution ground-penetrating radar, through-wall imaging, precision navigation and asset tracking, just to name a few. This tutorial focuses on UWB wireless communications at the physical layer. It overviews the state-of-the-art in channel modeling, transmitters, and receivers of UWB radios, and outlines research directions and challenges to be overcome. As signal processing expertise is expected to have major impact in research and development of UWB systems, emphasis is placed on DSP aspects.

Introduction

UWB characterizes transmission systems with instantaneous spectral occupancy in excess of 500 MHz

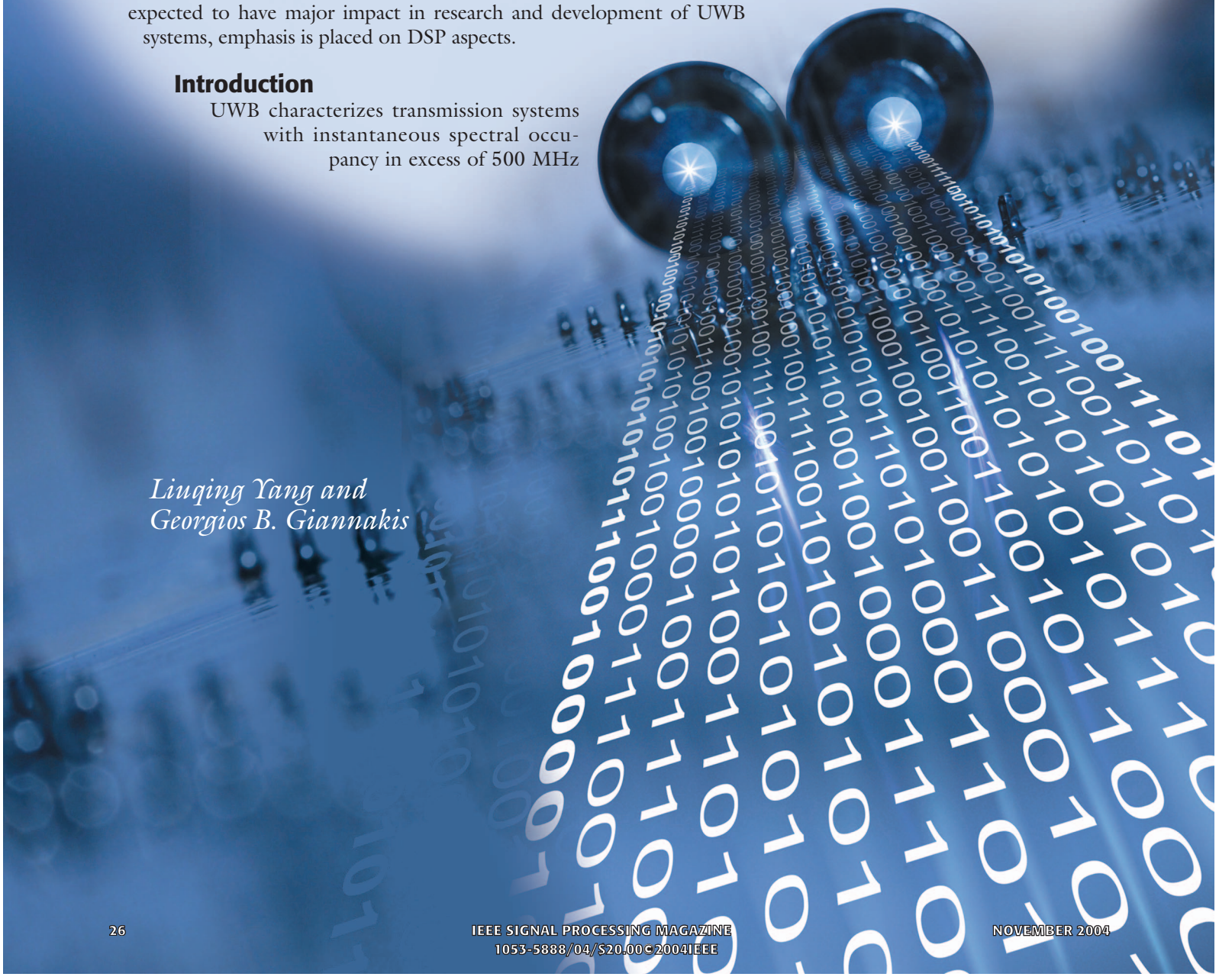

Liuqing Yang and Georgios B. Giannakis

1053-5888/04/$20.00©2004IEEE

or a fractional bandwidth of more than 20%. (The fractional bandwidth is defined as B/f_c, where $B := f_H - f_L$ denotes the -10 dB bandwidth and center frequency $f_c := (f_H + f_L)/2$ with f_H being the upper frequency of the -10 dB emission point, and f_L the lower frequency of the -10 dB emission point. According to [12], UWB systems with $f_c > 2.5$ GHz need to have a -10 dB bandwidth of at least 500 MHz, while UWB systems with $f_c < 2.5$ GHz need to have fractional bandwidth at least 0.20.) Such systems rely on ultra-short (nanosecond scale) waveforms that can be free of sine-wave carriers and do not require IF processing because they can operate at baseband. As information-bearing pulses with ultra-short duration have UWB spectral occupancy, UWB radios come with *unique advantages* that have long been appreciated by the radar and communications communities: i) enhanced capability to penetrate through obstacles; ii) ultra high precision ranging at the centimeter level; iii) potential for very high data rates along with a commensurate increase in user capacity; and iv) potentially small size and processing power. Despite these attractive features, interest in UWB devices prior to 2001 was primarily limited to radar systems, mainly for military applications. With bandwidth resources becoming increasingly scarce, UWB radio was "a midsummer night's dream" waiting to be fulfilled. But things changed drastically in the spring of 2002, when the FCC released a spectral mask allowing (even commercial) operation of UWB radios at the noise floor, but over an enormous bandwidth (up to 7.5 GHz).

This huge "new bandwidth" opens the door for an unprecedented number of bandwidth-demanding position-critical low-power applications in wireless communications, networking, radar imaging, and localization systems [64]. It also explains the rapidly increasing efforts undertaken by several research institutions, industry, and government agencies to assess and exploit the potential of UWB radios in various areas. These include short-range, high-speed access to the Internet, accurate personnel and asset tracking for increased safety and security, precision navigation, imaging of steel reinforcement bars in concrete or pipes hidden inside walls, surveillance, and medical monitoring of the heart's actual contractions.

For wireless communications in particular, the FCC regulated power levels are very low (below -41.3 dBm), which allows UWB technology to overlay already available services such as the global positioning system (GPS) and the IEEE 802.11 wireless local area networks (WLANs) that coexist in the 3.6–10.1 GHz band. Although UWB signals can propagate greater distances at higher power levels, current FCC regulations enable high-rate (above 110 MB/s) data transmissions over a short range (10–15 m) at very low power. Major efforts are currently under way by the IEEE 802.15 Working Group for standardizing UWB wireless radios for indoor (home and office) multimedia transmissions. Similar to the frequency reuse principle exploited by wireless cellular architectures, low-power, short-range UWB communications are also potentially capable of providing high spatial capacity, in terms of bits per second per square meter. In addition, UWB connectivity is expected to offer a rich set of software-controllable parameters that can be used to design location-aware communication networks flexible to scale in rates and power requirements.

To fulfill these expectations, however, UWB research and development has to cope with formidable challenges that limit their bit error rate (BER) performance, capacity, throughput, and network flexibility. Those include high sensitivity to synchronizing the reception of ultra-short pulses, optimal exploitation of fading propagation effects with pronounced frequency-selectivity, low-complexity constraints in decoding high-performance multiple access protocols, and strict power limitations imposed by the desire to minimize interference among UWB communicators, and with coexisting legacy systems, particularly GPS, unmanned air vehicles (UAVs), aircraft radar, and WLANs. These challenges call for advanced digital signal processing (DSP) expertise to accomplish tasks such as synchronization, channel estimation and equalization, multiuser detection, high-rate high-precision low-power analog/digital conversion (ADC), and suppression of aggregate interference arising from coexisting legacy systems. As DSP theory, algorithms, and hardware advanced narrowband and broadband technology, DSP is expected to play a similar role in pushing the frontiers of emerging UWB applications. To this end, it is important to understand features and challenges that are unique to UWB signaling from a DSP perspective.

Regulatory Issues and Motivating Applications

Despite its renewed interest during the past decade, UWB has a history as long as radio. When invented by Guglielmo Marconi more than a century ago, radio communications utilized enormous bandwidth as information was conveyed using spark-gap transmitters. The next milestone of UWB technology came in the late 1960s, when the high sensitivity to scatterers and low power consumption motivated the introduction of UWB radar systems [5], [45], [46]. Ross' patent in 1973 set up the foundation for UWB communications. Readers are referred to [5] for an interesting and informative review of pioneer works in UWB radar and communications.

In 1989, the U.S. Department of Defense (DoD) coined the term "ultra wideband" for devices occupying at least 1.5 GHz, or a -20 dB fractional bandwidth exceeding 25% [37]. Similar definitions were also adopted by the FCC notice of proposed rule making that regulated UWB recently. The rule making of UWB was opened by FCC in 1998. The resulting First Report and Order (R&O) that permitted deployment

of UWB devices was announced on 14 February and released in April 2002 [12]. Three types of UWB systems are defined in this R&O: imaging systems, communication and measurement systems, and vehicular radar systems. Spectral masks assigned to these applications are listed in Table 1. In particular, the FCC assigned bandwidth and spectral mask for indoor communications is illustrated in Figure 1.

Although currently only the United States permits operation of UWB devices, regulatory efforts are under way both in Europe and in Japan. Market drivers for UWB technology are many even at this early stage, and are expected to include new applications in the next few years. We outline here application trends where signal processing tools will probably have considerable impact in UWB system development.

▲ *Wireless personal area networks (WPANs):* Also known as in-home networks, WPANs address short-range (generally within 10–20 m) ad hoc connectivity among portable consumer electronic and communication devices. They are envisioned to provide high-quality real-time video and audio distribution, file exchange among storage systems, and cable replacement for home entertainment systems. UWB technology emerges as a promising physical layer candidate for WPANs, because it offers high-rates over short range, with low cost, high power efficiency, and low duty cycle.

▲ *Sensor networks:* Sensor networks consist of a large number of nodes spread across a geographical area. The nodes can be static, if deployed for, e.g., avalanche monitoring and pollution tracking, or mobile, if equipped on soldiers, firemen, or robots in military and emergency response situations. Key requirements for sensor networks operating in challenging environments include low cost, low power, and multifunctionality. High data-rate UWB communication systems are well motivated for gathering and disseminating or exchanging a vast quantity of sensory data in a timely manner. Typically, energy is more limited in sensor networks than in WPANs because of the nature of the sensing devices and the difficulty in recharging their batteries. Studies have shown that current commercial Bluetooth devices are less suitable for sensor network applications because of their energy requirements [62] and higher expected cost [2]. In addition, exploiting the precise localization capability of UWB promises wireless sensor networks with improved positioning accuracy. This is especially useful when GPSs are not available, e.g., due to obstruction.

▲ *Imaging systems:* Different from conventional radar systems where targets are typically considered as point scatterers, UWB radar pulses are shorter than the target dimensions. UWB reflections off the target exhibit not only changes in amplitude and time shift but also changes in the pulse shape. As a result, UWB waveforms exhibit pronounced sensitivity to scattering relative to conventional radar signals. This property has been readily adopted by radar systems (see e.g., [5] and references therein) and can be extended to additional applications, such as underground, through-wall and ocean imaging, as well as medical diagnostics and border surveillance devices [55], [57].

▲ *Vehicular radar systems:* UWB-based sensing has the potential to improve the resolution of conventional proximity and motion sensors. Relying on the high ranging accuracy and target differentiation capability enabled by UWB, intelligent collision-avoidance and cruise-control systems can be envisioned. These systems can also improve airbag deployment and adapt suspension/braking systems depending on road conditions. UWB technology can also be integrated into vehicular entertainment and navigation systems by downloading high-rate data from airport off ramp, road-side, or gas station UWB transmitters.

Table 1. FCC spectral mask for UWB systems.

	Equivalent Isotropically Radiated Power (EIRP) [dBm]					
Frequency [MHz]	**Indoor Comm.**	**Hand Held Comm.**	**Low Freq. Imaging**	**High Freq. Imaging**	**Med. Freq. Imaging**	**Vehicular Radar**
<960	15.209 limits	15.209 limits	15.209 limits	15.209 limits	15.209 limits	15.209 limits
960–1610	–75.3	–75.3	–65.3	–65.3	–53.3	–75.3
1610–1900	–53.3	–63.3	–53.3	–53.3	–51.3	
1900–1990		–61.3				
1990–3100	–51.3			–51.3	–41.3	–61.3
3100–10,600	–41.3	–41.3		–41.3		
10,600–22,000			–51.3			
22,000–29,000	–51.3	–61.3		–51.3	–51.3	–41.3
20,000–31,000						–51.3
>31,000						–61.3

Indoor/handled communication systems: $f_L, f_H \in [3.1, 10.6]$ GHz; low-frequency imaging systems: $f_L, f_H < 960$ MHz; high-frequency imaging systems: $f_L, f_H \in [3.1, 10.6]$ GHz; medium-frequency imaging systems: $f_L, f_H \in [1.99, 10.6]$ GHz; vehicular radar systems: $f_c > 24.075$ GHz, $f_L, f_H \in [22, 29]$ GHz.

UWB Communications at the Physical Layer

In this section, we outline physical layer issues of UWB communication systems, including transmitter/receiver designs, synchronization, channel estimation, and multiple access schemes. In addition to the conventional single-band UWB transmissions, we will also discuss recent multiband alternatives for power-efficient adherence to FCC's spectral mask, mitigation of narrowband interference (NBI), and relaxed sampling requirements. To appreciate UWB system designs, however, it is important to understand first the propagation characteristics of the transmitted ultra-short waveform and establish a realistic channel model.

Channel Modeling

Since more than 80% of the envisioned commercial UWB applications will be indoor communications, we will focus on indoor channels. The well-known Saleh-Valenzuela (S-V) indoor channel model was established back in 1987 [50], based on measurements utilizing low power ultra-short pulses (of width 10 ns and center frequency 1.5 GHz) in a medium-size, two-story office building. In the S-V model, multipath components arrive at the receiver in groups (clusters). Cluster arrivals are Poisson distributed with rate Λ. Within each cluster, subsequent arrivals are also Poisson distributed with rate $\lambda > \Lambda$. With $\alpha_{m,n}$ denoting the gain of the nth multipath component of the mth cluster, having phase $\theta_{m,n}$, the channel impulse response can be expressed as

$$h(t) = \sum_{l=0}^{+\infty} \alpha_l \delta(t - \tau_l) = \sum_{m=0}^{+\infty} \sum_{n=0}^{+\infty} \alpha_{m,n} e^{j\theta_{m,n}} \delta(t - T_m - \tau_{m,n}), \quad (1)$$

where $T_m + \tau_{m,n}$ ($\tau_{m,0} = 0$) denotes the arrival time of the nth multipath component of the mth cluster, $\theta_{m,n}$ are independent uniform random variables over $[0, 2\pi)$, and $\alpha_{m,n}$ are independent Rayleigh random variables with power $\mathrm{E}\{\alpha_{m,n}^2\} = \mathrm{E}\{\alpha_{0,0}^2\} e^{-T_m/\gamma} e^{-\tau_{m,n}/\gamma}$, where $\Gamma > \gamma$. The number of clusters and multipath components may theoretically extend over infinite time. However, the terms of the double sum in (1) practically vanish for sufficiently large (m, n) with an exponentially decaying power profile.

Lately, efforts have been made to characterize UWB channels with bandwidths exceeding 2 GHz. To come up with a statistical model, channel realizations are identified either in the frequency domain by frequency sweeping or in the time domain using impulsive signals. In November 2002, the channel modeling subcommittee of the IEEE 802.15.3a Task Group recommended a channel model which captures the aforementioned works, as well as recent refinements [14]. Because the clustering phenomenon has been experimentally confirmed, the standardized channel model is basically a modified version of the S-V model [50]. To reach an analytically tractable channel model, the total number of paths is defined as the number of multipath arrivals with expected power within 10 dB from that of the strongest arrival. The Rayleigh distribution in the S-V channel model is replaced by the log-normal distribution. The phases $\theta_{m,n}$ are also constrained to take values 0 or π with equal probability to account for signal inversion due to reflection, yielding a *real-valued* channel model. With path gains normalized to have unit energy, a log-normal random variable is introduced to account for shadowing. Model parameters corresponding to several ranges are also provided in [14], for both line-of-sight (LOS) and nonline-of-sight (NLOS) scenarios. The standardized UWB channel model in [14] is claimed to better match the measurements. However, the log-normal distribution and the shadowing factor render this model less tractable for theoretical performance analysis and quantification of the channel-induced diversity and coding gains.

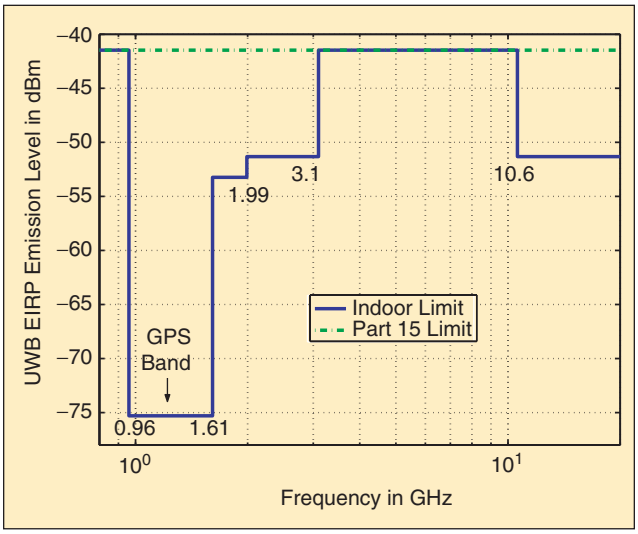

▲ *1. FCC spectral mask for indoor commercial systems.*

A typical realization of the channel impulse response generated using the channel model 2 [14] is shown in Figure 2. The number of multipath components is 315 in this realization, spanning over a delay spread of about 50 ns. Let $p(t)$ denote the transmitted pulse of duration T_p. After multipath propagation, the received waveform is given by the convolution of $p(t)$ with the physical channel $h(t)$, and contains multiple delayed copies of $p(t)$; i.e., $g(t) := (p \star h)(t) = \sum_{l=0}^{L} \alpha_l p(t - \tau_l)$, where $\star$ denotes convolution. Notice from Figure 2 that the spacing among multipath delays $\{\tau_l\}_{l=0}^{L}$ is in the order of nanoseconds. These delayed copies of $p(t)$ in $g(t)$ can be resolved from each other only if T_p is sufficiently small, that is, if the transmit bandwidth $B \approx 1/T_p$ is sufficiently large. The transmitted and received waveforms corresponding to two T_p values are shown in Figure 3, where the received waveforms were generated using the multipath delays and amplitudes of Figure 2.

With $T_p = 91$ ns, we have $B \approx 11$ MHz, and the received waveform consists of a single distorted version of $p(t)$. With $T_p = 0.55$ ns, we have $B \approx 2$ GHz, and the received waveform contains multiple resolvable copies of $p(t)$. If the channel is known at the receiver, these resolvable copies can be combined coherently to provide multipath diversity. But before discussing receiver designs that collect this diversity, let us first introduce UWB transmission schemes.

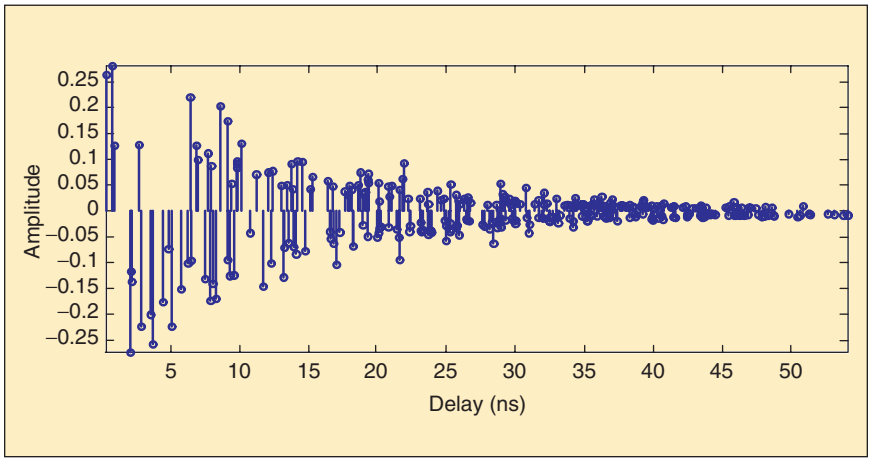

▲ *2. A typical realization of the channel impulse response generated using the IEEE 802.15.3 a channel model 2: NLOS channels with 0–4 m transmitter-receiver distance.*

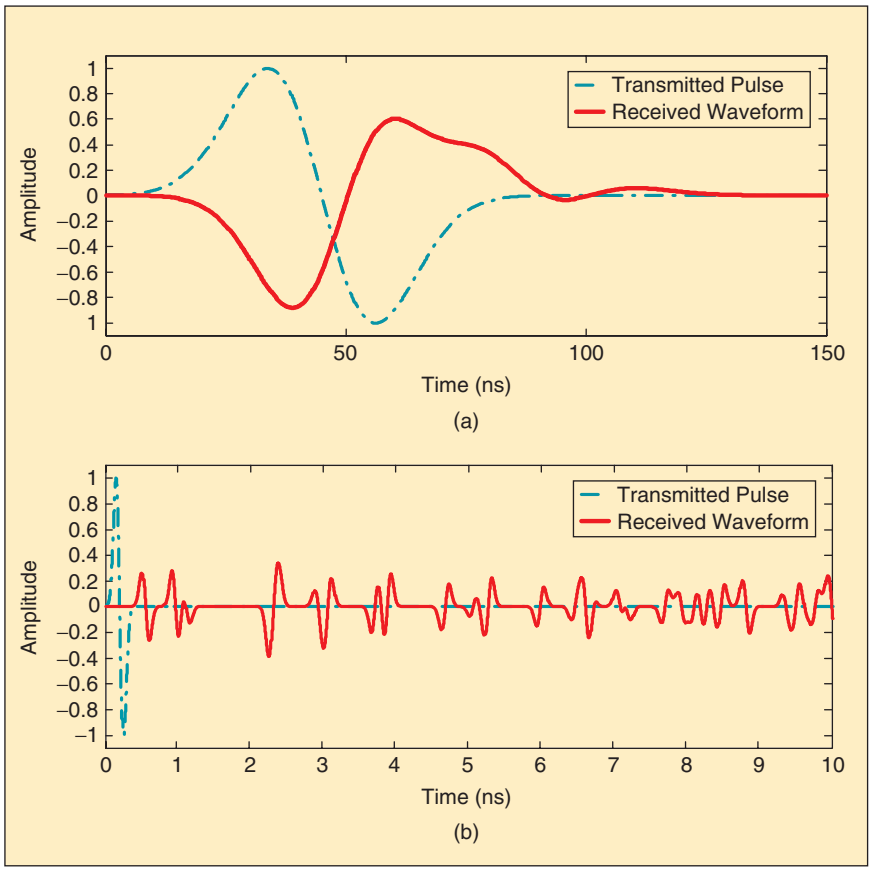

▲ *3. The transmitted and received waveforms corresponding to (a) $T_p = 91$ ns and (b) $T_p = 0.55$ ns. For illustration purposes, only the first 10 ns are shown in (b).*

Transmitter Design

Generally adopted spectrum shapers $p(t)$ for UWB communications include the Gaussian pulse, the Gaussian monocycle (first derivative of Gaussian pulse), and the second derivative of the Gaussian pulse, as depicted in Figure 4, along with their Fourier transforms (FTs). The reason behind the popularity of these pulses is twofold: i) Gaussian pulses come with the smallest possible time-bandwidth product of 0.5, which maximizes range-rate resolution and ii) the Gaussian pulses are readily available from the antenna pattern [51]. With T_p at the subnanosecond scale, $p(t)$ occupies UWB with bandwidth $B \approx 1/T_p$. As mentioned before, and illustrated in Figure 3(b), such an ultra-short $p(t)$ also gives rise to multiple resolvable copies, and thus enables rich multipath diversity.

In a typical UWB system, each information-conveying symbol is represented by a number of (N_f) pulses, each transmitted per frame of duration $T_f \gg T_p$. Having N_f frames, over which a single symbol is spread, reverses the commonly used terminology where a frame consists of multiple symbols (here multiple frames comprise a symbol). With M-ary modulation, $\log_2 M$ message bits are transmitted during a signaling interval of duration $T_s = N_f T_f$ s that corresponds to a bit rate $R_b = \log_2 M/T_s$.

Being real, baseband UWB transmissions neither have to entail frequency modulation nor phase modulation with $M > 2$. Consequently, symbol values can be transmitted by modulating the position and/or the amplitude of $p(t)$. In M-ary pulse position modulation (PPM), M distinctly delayed pulses $\{p(t - \Delta_m)\}_{m=0}^{M-1}$ are employed, each representing one symbol value. Generally, the so-termed modulation indices Δ_m are chosen such that $\Delta_m = m\Delta$ with $\Delta \geq T_p$, which corresponds to an orthogonal PPM. In binary PPM, the delay Δ can also be chosen to minimize the correlation $\int p(t)p(t - \Delta)dt$ [52]. As bandwidth efficiency drops with increasing modulation size M, PPM is suitable for power-limited applications. In fact, PPM was almost exclusively adopted in the early

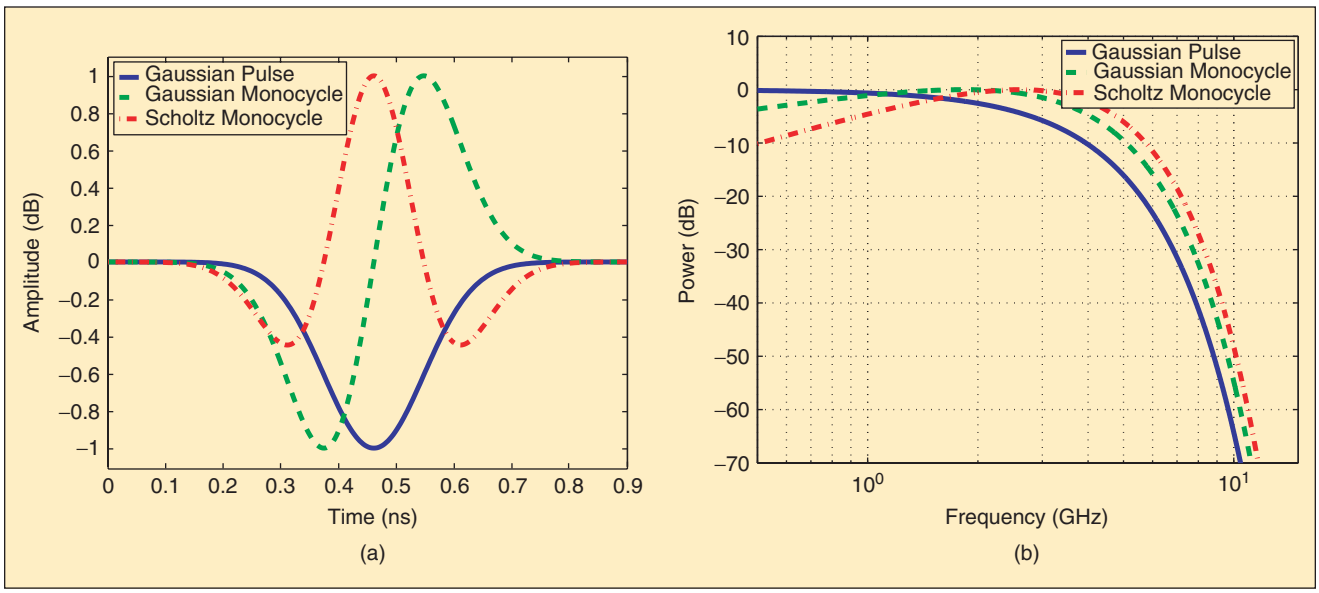

▲ *4. (a) Generally adopted pulse shapes in UWB communications; (b) Fourier transform of several pulse shapes. Pulse width:* 0.7 *ns.*

development of UWB radios because negating ultra-short pulses were difficult to implement. Another modulation scheme that does not require pulse negation is the so termed on-off keying (OOK), where symbol "1" is represented by transmitting a pulse, and "0" by transmitting nothing.

As pulse negation became easier to implement, pulse amplitude modulation (PAM) attracted more attention. In particular, when $M = 2$, antipodal pulses are used to represent binary symbols, as in binary phase shift keying (BPSK) or bipolar signaling. Biorthogonal signaling by combining orthogonal PPM with binary PAM as well as orthogonal waveform and block orthogonal modulation schemes have also been reported [43].

To allow for multi-user access (MA) to the UWB channel, time hopping (TH) was introduced early in [52]. With TH, each pulse is positioned within each frame duration T_f according to a user-specific TH sequence $c_u^{TH}(n)$. Specifically, dividing each frame into N_c chips each of duration T_c, the uth user's TH code $c_u^{TH}(n) \in [0, N_c - 1]$ corresponds to a time shift of $c_u^{TH}(n)T_c$ during the nth frame [72]. Consequently, the uth user's transmitted waveform is given by

$$v_u(t) = \sqrt{\mathcal{E}_u} \sum_{n=0}^{+\infty} a_u\left(\lfloor n/N_f \rfloor\right) \cdot p\left(t - nT_f - c_u^{\mathrm{TH}}(n)T_c - b_u\left(\lfloor n/N_f \rfloor\right)\Delta\right), \tag{2}$$

where $\mathcal{E}_u$ is the uth user's energy per pulse at the transmitter end. With $s_u(k) \in [0, M-1]$ denoting the M-ary information symbol transmitted by the uth user during the kth symbol duration, (2) subsumes several modulation schemes. When $b_u(k) = s_u(k)$, and $a_u(k) = 1$, (2) describes UWB transmissions with M-ary PPM; when $a_u(k) = 2s_u(k) + 1 - M$, and $b_u(k) = 0$, (2) models M-ary PAM. With binary symbols, and $b_u(k) = 0$, $a_u(k) = 2s_u(k) - 1$ corresponds to BPSK, and $a_u(k) = s_u(k)$ corresponds to OOK [32], [43], [69].

With TH codes, MA is achieved by altering the pulse *position* from frame to frame, according to the sequence $c_u^{\mathrm{TH}}(n)$. MA can also be enabled by modifying the pulse *amplitude* from frame to frame. The latter allows for many other choices of alternative spreading codes which, individually or in combination with TH codes, give rise to the following transmitted waveform [c.f. (2)]:

$$v_u(t) = \sqrt{\mathcal{E}_u} \sum_{n=0}^{+\infty} a_u\left(\lfloor n/N_f \rfloor\right) c_u(n) \cdot p\left(t - nT_f - c_u^{\mathrm{TH}}(n)T_c - b_u\left(\lfloor n/N_f \rfloor\right)\Delta\right), \tag{3}$$

where $c_u(n)$ is the user-specific "amplitude code" during the nth frame. Depending on the spreading codes employed, the UWB systems are termed TH-UWB [52], direct-sequence (DS)-UWB [15], or baseband single-carrier/multicarrier (SC/MC)-UWB [66], [77], just to name a few.

In addition to facilitating multiple access, spreading codes also shape the transmit spectrum. Analytical expressions and simulated power spectral density (PSD) for UWB transmissions are pursued in [44] and [70]. A PSD expression for TH-UWB allowing for both short and long spreading codes is derived in [44]. The effects of timing jitter on PSD of UWB transmissions utilizing random TH codes and/or M-ary modulation can be found in [70]. In particular, let us consider "short" spreading codes that are symbol-periodic with period N_f. Let us now define the symbol level transmitted waveform for user u as

$p_{T,u}(t) := \sum_{n=0}^{N_f-1} p(t - nT_f - c_u^{\mathrm{TH}}(n)T_c)$ for TH-UWB, $p_{T,u}(t) := \sum_{n=0}^{N_f-1} c_u(n)p(t - nT_f)$ for DS/SC/MC-UWB, and $p_{T,u}(t) := \sum_{n=0}^{N_f-1} p(t - nT_f)$ when no spreading code is involved. Equation (2) then becomes $v_u(t) = \sqrt{\mathcal{E}_u}\sum_{k=0}^{+\infty} a_u(k)p_{T,u}(t - kT_s - b_u(k)\Delta)$. Along the lines of [42, Chapter 4], it can be shown that the PSD of $v_u(t)$ is

$$\Phi_{vv}(f) = \frac{\mathcal{E}_u}{T_s}|P_{T,u}(f)|^2 \sum_{n=-\infty}^{\infty} \phi_{aa}^{(n)}\phi_{bb}^{(n)}(f)e^{-j2\pi f nT_s}, \quad (4)$$

where $\phi_{aa}^{(n)} := \mathrm{E}\{a_u(k)a_u(k+n)\}$, $\phi_{bb}^{(n)}(f) := \mathrm{E}\{e^{-j2\pi f(b_u(k)-b_u(k+n))\Delta}\}$, and $P_{T,u}(f) := \mathcal{F}\{p_{T,u}(t)\}$ is the FT of $p_{T,u}(t)$. In particular, for independent identically distributed (i.i.d.) equiprobable binary symbols $s_u(k) \in \{0, 1\}$, we have $a_u(k) = 2s_u(k)-1$, and $b_u(k) = 0$ with PAM; and $a_u(k) = 1$, and $b_u(k) = s_u(k)$ with PPM. It then follows that

$$\phi_{aa}^{(n)} = \delta(n), \quad \text{and} \quad \phi_{bb}^{(n)}(f) = 1, \quad \forall n$$

for binary PAM and

$$\phi_{aa}^{(n)} = 1, \forall n, \quad \text{and} \quad \phi_{bb}^{(n)}(f) = \begin{cases} 1, & n = 0 \\ \dfrac{1+\cos(2\pi\Delta f)}{2}, & n \neq 0 \end{cases}$$

for binary PPM. Accordingly, the resultant PSD of $v_u(t)$ becomes [c.f. (4)]: $\Phi_{vv}(f) = (\mathcal{E}_u/T_s)|P_{T,u}(f)|^2$ for PAM and $\Phi_{vv}(f) = (\mathcal{E}_u/T_s)|P_{T,u}(f)|^2[(1-\cos(2\pi\Delta f))/2 + (1+\cos(2\pi\Delta f))/(2T_s)\sum_{n=-\infty}^{\infty}\delta(f - k/T_s)]$ for PPM.

The shape of the $\Phi_{vv}(f)$ for both modulations is determined by $P_{T,u}(f)$, which may contain spectral lines due to the repeated use of N_f pulses in forming each symbol. Different from PAM, which is a zero-mean linear modulation, additional spectral lines

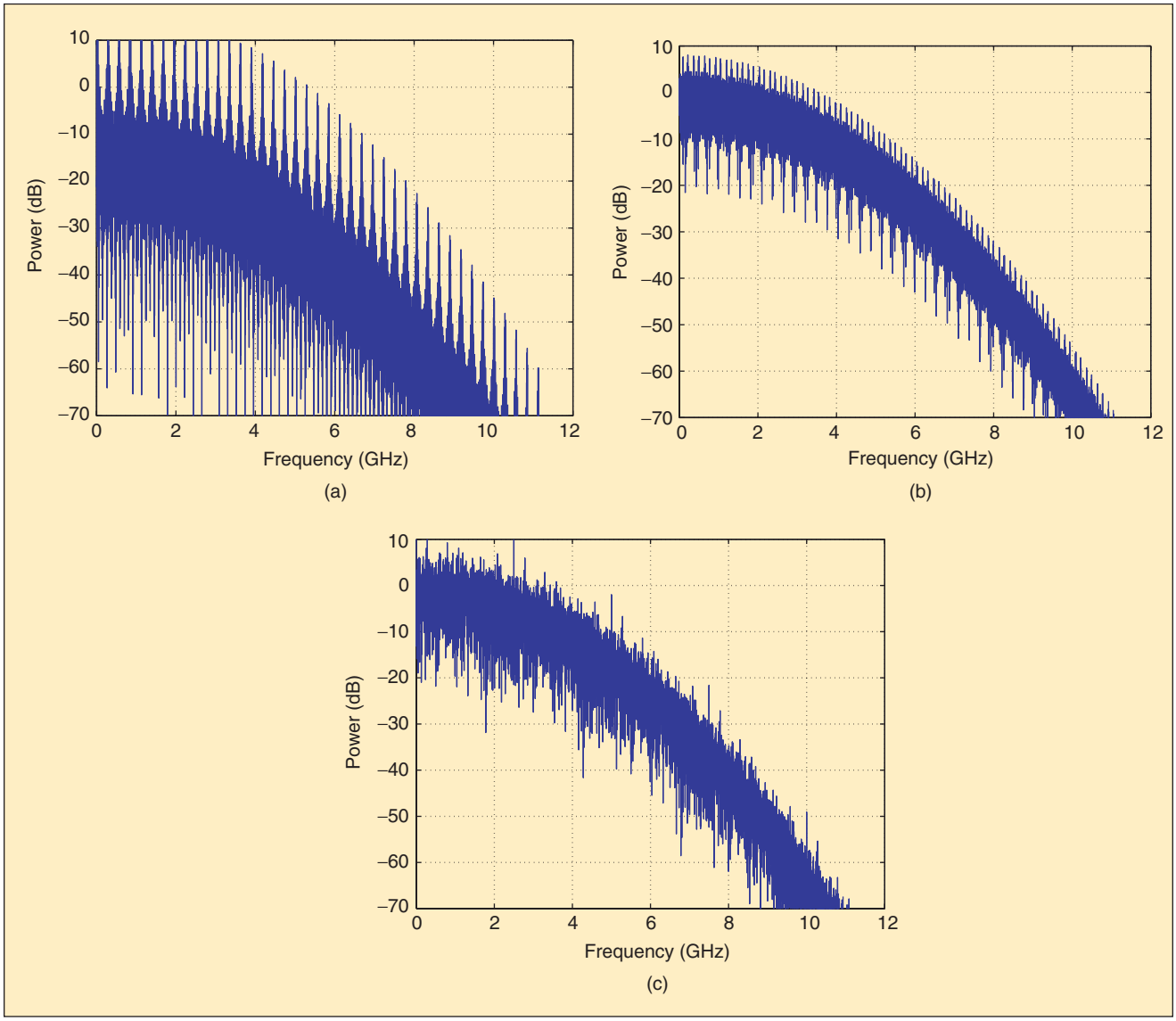

▲ *5. Transmit PSD corresponding to (a) no spreading code, (b) random DS codes, and (c) random TH codes. Gaussian pulse with* $T_p = 0.4$ *ns.* $N_f = 64$, $T_f = 100$ *ns,* $T_c = 2$ *ns.*

emerge with PPM. Although the bandwidth of $P_{T,u}(f)$ is determined by the pulse shaper $p(t)$, its shape, by definition, relies not only on $p(t)$, but also on the spreading codes utilized. The transmit PSD corresponding to no spreading, random DS spreading, and random TH spreading with binary PAM are depicted in Figure 5. Notice how pronounced spectral lines are in Figure 5 where no spreading code is used. Figure 5(b) and (c) confirms that both DS and TH spreading smooth the transmit PSD. It is also worth mentioning that although the spectral lines cause "noise-like" interference to narrowband services coexisting with UWB systems, they introduce cyclostationarity that one can exploit for timing offset estimation simply because these spectral lines originate from the underlying periodicity of the transmission.

Timing Synchronization

As defined in (1), the physical channel $h(t)$ not only captures multipath effects but also includes a delay (uncertainty) on the first arrival time τ_0. For coherent demodulation, timing synchronization is the first task to be performed at the receiver to acquire and track the timing offset τ_0.

In fact, one of the major challenges at the UWB physical layer is the accuracy and speed of this synchronization step. As UWB systems employ low-power ultra-short pulses (in the order of nanoseconds), timing requirements are stringent because even minor misalignments may result in lack of energy capture which renders symbol detection impossible [59]. To better understand the unique challenges in UWB timing, let us consider a single-user link with zero-mean, i.i.d. M-ary PAM symbols $a(k)$ having zero-mean and variance σ_s^2. (Generalization to PPM is also possible.) Dropping temporarily the subscript u, the received signal after multipath propagation is [c.f. (3)]: $r(t) = \sqrt{\mathcal{E}} \sum_{k=0}^{\infty} a(k) \sum_{l=0}^{L} \alpha_l p_T(t - kT_s - \tau_l) + \eta(t)$, where $(L+1)$ is the number of effectively nonzero paths, each with amplitude α_l and delay τ_l satisfying $\tau_l < \tau_{l+1}$, $\forall l$. We assume that the channel is quasi-static, meaning that $\{\alpha_l\}_{l=0}^{L}$ and $\{\tau_l\}_{l=0}^{L}$ remain invariant per burst but may change from burst to burst; $a(k)$, $\{\alpha_l\}_{l=0}^{L}$ and $\{\tau_l\}_{l=0}^{L}$ are independent of the noise $\eta(t)$ which is assumed zero-mean, wide-sense stationary but not necessarily white and/or Gaussian, as it consists of both ambient noise and multi-user interference (MUI). With respect to the first arrival time (timing offset) τ_0, other path delays can be uniquely described as: $\tau_{l,0} := \tau_l - \tau_0$, $\forall l \in [0, L]$. It is convenient to express $r(t)$ in terms of the *aggregate pulse* $p_R(t)$ at the receiver which encompasses the transmit pulse, spreading codes and multipath effects:

$$r(t) = \sqrt{\mathcal{E}} \sum_{k=0}^{\infty} a(k) p_R(t - kT_s - \tau_0) + \eta(t),$$

where

$$p_R(t) := \sum_{l=0}^{L} \alpha_l p_T(t - \tau_{l,0}). \tag{5}$$

Let us select $T_f \geq \tau_{L,0} + T_p$ and $c^{\mathrm{TH}}(0) \geq c^{\mathrm{TH}}(N_f - 1)$ to confine the duration of $p_R(t)$ within $[0, T_s)$ and thus avoid intersymbol interference (ISI). Without loss of generality, let us also confine the timing offset τ_0 within a symbol duration, i.e., $\tau_0 \in [0, T_s)$.

Notice that at the timing synchronization stage, the multipath channel is unknown, and so is $p_R(t)$. Consequently, even with known training symbols $a(k)$, the traditional approach of peak-picking the correlation of $r(t)$ with $p_R(t)$ to estimate τ_0 is not applicable. Instead of $p_R(t)$, one could correlate $r(t)$ with $p_T(t)$ and look for the maximum. Evidently, this approach is not only suboptimum in the presence of dense multipath, but also results in unacceptably slow acquisition speed and has prohibitive complexity when one has to perform exhaustive search over thousands of bins/chips. There is clearly a need for low-complexity timing estimation methods in multipath-rich propagation settings. To this end, a number of attempts have been proposed to improve acquisition speed and/or performance in UWB radios. These attempts include: a coarse bin reversal search for the noiseless case [22]; a coded beacon sequence in conjunction with a bank of correlators in the context of data-aided localization in the absence of multipath [13]; a ranging system that requires knowledge of the strongest path [26]; a non-data aided (a.k.a. blind) timing estimator that relies on the cyclostationarity that arises in UWB transmissions with slow TH and sufficiently dense multipath [61]; and a data-aided maximum likelihood (ML) timing algorithm using symbol- and frame-rate samples [60].

UWB Timing with Dirty Templates

To relax the rather restrictive assumptions in these approaches, we have developed timing algorithms based on the novel concept of "dirty templates" [79]. The idea is to rely on pairs of successive symbol-long segments of $r(t)$ taken at candidate time-shifts $\tau \in [0, T_s)$ and have one segment in each pair serve as a template for the other. Specifically, integrate-and-dump operations are performed on products of such segments to obtain *symbol-rate* samples:

$$x_k(\tau) = \int_0^{T_s} r(t + kT_s + \tau) r(t + (k-1)T_s + \tau)\, dt, \tag{6}$$

$\forall k \in [1, +\infty)$ and $\tau \in [0, T_s)$. The symbol-long segments $r(t + kT_s + \tau)$ and $r(t + (k-1)T_s + \tau)$, for $t \in [0, T_s)$ are "dirty templates" because: i) they are noisy, ii) they are distorted by the *unknown* channel, and iii) they are subject to the *unknown* offset τ_0. The latter

UWB characterizes transmission systems with instantaneous spectral occupancy in excess of 500 MHz or a fractional bandwidth of more than 20%.

constitutes a major difference between the Timing technique based on dirty templates (TDT) and the transmitted reference (TR) approach [21] for channel estimation and symbol demodulation, as we will detail in the ensuing sections. To grasp the gist of TDT, let $\bar{x}_k(\tau)$ and $\bar{r}(t)$ denote the noise-free parts of $x_k(\tau)$ and $r(t)$. Applying Cauchy-Schwartz's inequality to (6) yields

$$\bar{x}_k^2(\tau) \le \int_0^{T_s} \bar{r}^2(t+kT_s+\tau)\,dt \times \int_0^{T_s} \bar{r}^2(t+(k-1)T_s+\tau)\,dt,$$

where the equality holds $\forall k$ if and only if $\bar{r}(t+kT_s+\tau) = \lambda \bar{r}(t+(k-1)T_s+\tau)$. But the latter is true $\forall t \in [0, T_s)$ if and only if $\tau = \tau_0$. In words, the cross correlation of successive symbol-long received segments reaches a *unique maximum* magnitude if and only if these segments are scaled versions of each other, which is achieved only at the correct timing; i.e., when $\tau = \tau_0$. In its simplicity, this neat observation offers a distinct criterion for timing synchronization that, for years, has relied on the idea that the autocorrelation of the noise-free template has a unique maximum at the correct timing; the latter has been the principle behind all existing narrowband and UWB timing schemes, including the popular early-late gate algorithm [42]. The TDT approach is different from these conventional synchronizers. It has fundamental implications to UWB and also to a number of other applications such as time-delay and displacement estimation through unknown time-dispersive media, where there is no undistorted template to rely on, even in the noise-free case.

To establish its validity even in the presence of noise, we start by recalling that $p_R(t)$ has finite nonzero support $[0, T_s)$. This implies that the noisy $x_k(\tau)$ can be expressed as [c.f. (5) and (6)]:

$$x_k(\tau) = a(k)\,[a(k-1)\mathcal{E}_A(\tilde{\tau}) + a(k+1)\mathcal{E}_B(\tilde{\tau})] + \xi(k), \tag{7}$$

where $\xi(k)$ denotes noise after correlation, $\mathcal{E}_A(\tilde{\tau}) := \mathcal{E}\int_{T_s-\tilde{\tau}}^{T_s} p_R^2(t)dt, \mathcal{E}_B(\tilde{\tau}) := \mathcal{E}\int_0^{T_s-\tilde{\tau}} p_R^2(t)dt$ and $\tilde{\tau} := (\tau_0 - \tau) \mod T_s$. The mean-square of $x_k(\tau)$ in (7) is $\mathrm{E}\{x_k^2(\tau)\} = \sigma_s^4[\mathcal{E}_A^2(\tilde{\tau}) + \mathcal{E}_B^2(\tilde{\tau})] + \sigma_\xi^2 = (\sigma_s^4/2) \times\{[\mathcal{E}_A(\tilde{\tau}) + \mathcal{E}_B(\tilde{\tau})]^2 + [\mathcal{E}_A(\tilde{\tau}) - \mathcal{E}_B(\tilde{\tau})]^2\} + \sigma_\xi^2$, where to cancel the cross terms in $x_k^2(\tau)$ we used that $\mathrm{E}\{a(k)a(l)\} = 0$ and $\mathrm{E}\{a^2(k)a^2(l)\} = \sigma_s^4$, for $k \neq l$. Now notice that $\mathcal{E}_A(\tilde{\tau}) + \mathcal{E}_B(\tilde{\tau}) = \int_0^{T_s} p_R^2(t)dt := \mathcal{E}_R$ is the constant energy of the unknown aggregate template at the receiver and also that $\mathcal{E}_B(\tilde{\tau}) - \mathcal{E}_A(\tilde{\tau})$ is uniquely maximized at $\tilde{\tau} = 0$, since $\mathcal{E}_A(\tilde{\tau})$ is minimized at $\tilde{\tau} = 0$ and $\mathcal{E}_B(\tilde{\tau})$ is maximized at $\tilde{\tau} = 0$, by definition. So, $\mathrm{E}\{x_k^2(\tau)\}$ is maximized when $\tilde{\tau} = 0$, or equivalently, $\tau = \tau_0$. Compactly written, the approach for *nondata aided* TDT yields: $\tau_0 = \arg\max_{\tau\in[0,T_s)} \mathrm{E}\{x_k^2(\tau)\}$.

As usual, the ensemble mean must be replaced in practice by its consistent sample mean estimator obtained from K symbol-long pairs of received segments: $K^{-1}\sum_{k=1}^{K} x_{2k-1}^2(\tau)$. The number of samples K required for reliable estimation can be reduced markedly if a *data aided* approach is pursued [79]. The training sequence $\{a(k)\}$ for data-aided TDT comprises a repeated pattern $(s, s, -s, -s)$ with s being any M-ary PAM symbol. This pattern is particularly attractive because it simplifies (7) to $x_k(\tau) = (-1)^k s^2[-\mathcal{E}_A(\tilde{\tau}) + \mathcal{E}_B(\tilde{\tau})] + \xi(k)$. As a result, $K^{-1}\sum_{k=1}^{K} x_{2k-1}^2(\tau)$ converges faster to $\mathrm{E}\{x_k^2(\tau)\} = s^4[\mathcal{E}_A(\tilde{\tau}) - \mathcal{E}_B(\tilde{\tau})]^2 + \sigma_\xi^2$, because now one obviates convergence to σ_s^4, that is necessary in the blind approach to remove unknown symbol effects (self-noise). The benefit with data-aided TDT is very rapid acquisition since only $K = 1$ pair of received symbol-long segments carrying as few as four training symbols, is sufficient; see also Figure 6. Summarizing, consistent (non)data-aided TDT can be accomplished in the absence of ISI even when TH codes are present and the UWB multipath channel is unknown, using "dirty" T_s-long segments of the received waveform as follows [79]:

$$\hat{\tau}_0 = \arg\max_{\tau\in[0,T_s)} \sum_{k=1}^{K}\left(\int_{(2k-1)T_s}^{2kT_s} r(t+\tau)r(t+\tau-T_s)\,dt\right)^2. \tag{8}$$

Both training and blind modes have low-complexity as they require only symbol rate samples, but the data-aided mode enjoys also rapid acquisition relying on as few as four training symbols $[s, s, -s, -s]$.

The estimator in (8) enables timing synchronization at any desirable resolution constrained only by the affordable complexity: i) coarse timing with low complexity, e.g., by picking the maximum over N_f candidate offsets $\tau = nT_f$, where integer $n \in [0, N_f)$; ii) fine timing with higher complexity at the chip resolution with $\tau = iT_c$, $i \in [0, N_c)$; and iii) adaptive timing (tracking) with voltage-controlled clock (VCC) circuits; the preliminary tests in Figure 6 correspond to frame level timing resolution. As the TDT algorithms only require zero ISI, the condition $T_f \ge \tau_{L,0} + T_p$ can be relaxed to allow for higher data rates, as long as guard frames are inserted between symbols to avoid ISI, much like zero-padding in narrowband systems [67].

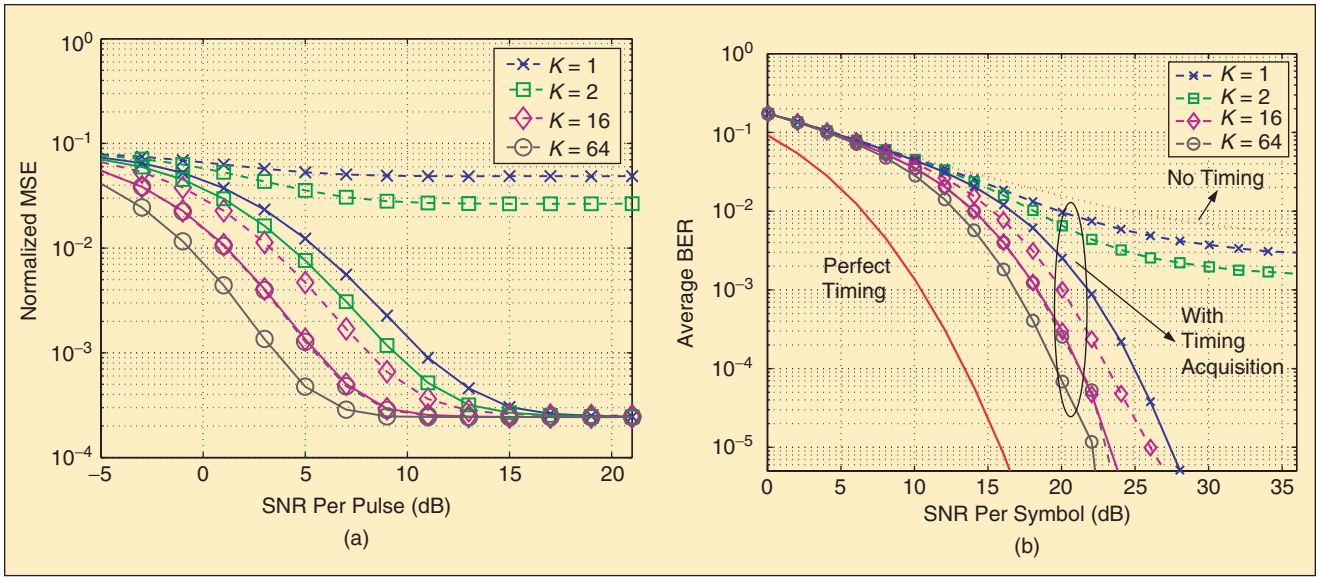

▲ 6. (a) Normalized MSE of $\hat{\tau}_0$ in (8) and (b) average BER using TDT algorithm. Dashed (solid) curves correspond to (non) data-aided mode.

Multi-User TDT

The timing algorithms we have introduced are for a peer-to-peer link where MUI is treated as noise. This is reasonable in a multi-user setting provided that user separability is ensured through channelization. But in such cases, user separation is sensitive to mistiming. To illustrate how data-aided TDT can be extended to a multi-user setup, suppose one wishes to synchronize to a single desired user (say user d) who is transmitting the training pattern $(s, s, -s, -s)$ and is received in the presence of other asynchronous users communicating information-bearing i.i.d. symbols. Equation (7) now becomes

$$\begin{aligned} x_k(\tau) &= \sum_{u=0}^{N_u-1} x_{u,k}(\tau) \\ &= \sum_{u=0}^{N_u-1} a_u(k)\,[a_u(k-1)\mathcal{E}_{u,A}(\tilde{\tau}_u) \\ &\qquad + a_u(k+1)\mathcal{E}_{u,B}(\tilde{\tau}_u)] + \xi(t), \end{aligned} \tag{9}$$

where $\mathcal{E}_{u,A}(\tilde{\tau}_u) := \mathcal{E}_u \int_{T_s-\tilde{\tau}_u}^{T_s} p_{u,R}^2(t)dt$, $\mathcal{E}_{u,B}(\tilde{\tau}_u) := \mathcal{E}_u \int_0^{T_s-\tilde{\tau}_u} p_{u,R}^2(t)dt$ and $\tilde{\tau}_u := (\tau_{u,0} - \tau) \mod T_s$ are as before, but with symbols, channels and offsets being user dependent. The desired user's samples at the dirty-template correlator output obey $x_{d,k}(\tau) = (-1)^k s^2[-\mathcal{E}_{d,A}(\tilde{\tau}_d) + \mathcal{E}_{d,B}(\tilde{\tau}_d)] + \xi(t)$. Upon averaging (without squaring), we obtain for the user under training $\mathrm{E}\{(-1)^k x_{d,k}(\tau)\} = s^2[\mathcal{E}_{d,B}(\tilde{\tau}_d) - \mathcal{E}_{d,A}(\tilde{\tau}_d)]$; while for all other users transmitting zero-mean i.i.d. symbols we have $\mathrm{E}\{(-1)^k x_{u,k}(\tau)\} = 0$. This observation suggests the following multi-user TDT estimator [c.f. (8)]

$$\hat{\tau}_{d,0} = \arg \max_{\tau\in[0,T_s)} \left[\sum_{k=1}^{K} (-1)^k \times \int_{kT_s}^{(k+1)T_s} r(t+\tau) r(t+\tau-T_s)\, dt \right]^2 .$$

Simulations indicate that this multi-user TDT scheme requires long training sequences. It is of interest to explore multi-user TDT algorithms that remain operational with short or even without training sequences.

Besides low-complexity timing algorithms that are operational in realistic UWB multi-user settings, analytical studies on system performance and capacity in the presence of timing errors are topics deserving further investigation. In the context of narrowband receivers, carrier synchronization and symbol timing issues have been investigated thoroughly [34]. Existing solutions include the spectral line generating synchronizers, the ML approach, and the cyclostationary approach. Performance is benchmarked using the (modified) Cramér-Rao bound (CRB) [34]. For wireless channels that are strongly frequency selective and quasi-static over time, recent developments in multicarrier modulation have stimulated renewed interest in synchronization. Considering the time-frequency duality between UWB and orthogonal frequency division multiplexing (OFDM) systems, these works may prove valuable in promoting a dual thrust for timing estimation of UWB signals. [This duality refers to the fact that OFDM conveys information via impulse-like signals in the frequency-domain (carriers), whereas a UWB system conveys information via impulse-like signals in the time-domain (ultra-short pulses).]

Upon synchronization, the receiver can adjust its timing according to the estimated first arrival time $\hat{\tau}_0$. In the following sections, we assume this estimate to be

perfect. Consequently, the multipath delays with respect to the adjusted receiver timing will be such that $\tau_0 = 0$.

Rake Reception and Multipath Diversity

The most commonly used UWB receiver is a correlation (matched filter) receiver [5], [52], where the received signal is correlated with the transmitted pulse $p(t)$. Conveying information with ultra-short pulses, UWB transmissions can resolve many paths, and are thus rich in multipath diversity (see Figure 3). This has motivated research towards designing correlation-based Rake receivers to collect the available diversity [8].

Frame- and Symbol-Rate Rake Receivers

For DS-, SC-, or MC-UWB systems with PAM modulation, the continuous-time received waveform is given by [c.f. (3)]

$$r_u(t) = v_u(t) \star h(t) + \eta(t) = \sqrt{\mathcal{E}_u} \sum_{n=0}^{\infty} a_u(\lfloor n/N_f \rfloor) c_u(n) g(t - nT_f) + \eta(t), \tag{10}$$

where $g(t) := (p \star h)(t) = \sum_{l=0}^{L} \alpha_l p(t - \tau_l)$ is the composite pulse-multipath channel. Since the frame duration T_f is up to our disposal, we can choose the frame duration longer than the maximum delay spread augmented by one pulse duration, i.e., $T_f \geq \tau_L + T_p$, to avoid interframe interference (IFI). Rake receivers with L_r fingers sum up weighted outputs (diversity combining) from a bank of L_r correlators. For clarity, we will consider correlation and diversity combining separately. During the nth frame, the template for the l_rth correlator (Rake finger with delay $\tilde{\tau}_{l_r}$) is the pulse $p(t)$ delayed by $nT_f + \tilde{\tau}_{l_r}$. Accordingly, the correlator output of the l_rth finger during the nth frame is

$$x_u(n; l_r) = \int_{nT_f + \tilde{\tau}_{l_r}}^{nT_f + \tilde{\tau}_{l_r} + T_p} r_u(t) p(t - nT_f - \tilde{\tau}_{l_r})\, dt. \tag{11}$$

Upon defining $\tilde{\alpha}_{l_r} := \int_{\tilde{\tau}_{l_r}}^{\tilde{\tau}_{l_r} + T_p} g(t) p(t - \tilde{\tau}_{l_r}) dt$, it follows that $\int_{nT_f + \tilde{\tau}_{l_r}}^{nT_f + \tilde{\tau}_{l_r} + T_p} g(t - mT_f) p(t - nT_f - \tilde{\tau}_{l_r}) dt = \tilde{\alpha}_{l_r} \delta(m - n)$, where to establish the latter, we used that $T_f > \tau_L + T_p$. Substituting (10) into (11), we find $x_u(n; l_r) = \sqrt{\mathcal{E}_u} a_u(\lfloor n/N_f \rfloor) c_u(n) \tilde{\alpha}_{l_r} + \eta(n; l_r)$, where $\eta(n; l_r)$ is the sampled noise, at the correlator output of the l_rth finger, during the nth frame. For each finger to capture distinct multipath returns, finger delays must satisfy $\tilde{\tau}_{l_r} - \tilde{\tau}_{l_r - 1} \geq 2T_p$, which yields the maximum number of fingers $\bar{L}_r := \lfloor \tau_L / (2T_p) \rfloor$. In practice, $L_r \leq \bar{L}_r$ is often chosen to trade off performance with complexity, leading to receiver options such as all Rake, partial Rake or selective Rake [71]. Notice that the filtered and sampled $\eta(n; l_r)$ stays white if the noise $\eta(t)$ is white, since $\tilde{\tau}_{l_r}$ are spaced sufficiently apart.

Concatenating the L_r outputs from all fingers during the nth frame we can form the block:

$$\boldsymbol{x}_u(n) := [x_u(n; 0)\ x_u(n; 1) \cdots x_u(n; L_r - 1)]^T = \sqrt{\mathcal{E}_u} a_u(\lfloor n/N_f \rfloor) c_u(n) \tilde{\boldsymbol{\alpha}} + \boldsymbol{\eta}(n), \tag{12}$$

where $\tilde{\boldsymbol{\alpha}}$ and $\boldsymbol{\eta}(n)$ are $L_r \times 1$ vectors constructed by stacking $\tilde{\alpha}_{l_r}$ and $\eta(n; l_r)$ for $l_r \in [0, L_r - 1]$. Recalling that each symbol is conveyed by N_f pulses, a total of $N_f L_r$ correlator outputs must be collected, L_r per frame, to decode one symbol. To this end, vectors $\{\boldsymbol{x}_u(n)\}_{n=kN_f}^{(k+1)N_f - 1}$ corresponding to the kth symbol can be concatenated into a vector of size $N_f L_r \times 1$ as [c.f. (12)]:

$$\boldsymbol{y}_u(k) := \left[\boldsymbol{x}_u^T(kN_f) \cdots \boldsymbol{x}_u^T(kN_f + N_f - 1)\right]^T = \sqrt{\mathcal{E}_u} a_u(k) (\boldsymbol{c}_u \otimes \tilde{\boldsymbol{\alpha}}) + \boldsymbol{\eta}(k), \tag{13}$$

where $\otimes$ stands for Kronecker product, $\boldsymbol{c}_u := [c_u(0), \ldots, c_u(N_f - 1)]^T$, and $\boldsymbol{\eta}(k) := [\boldsymbol{\eta}^T(kN_f), \ldots, \boldsymbol{\eta}^T(kN_f + N_f - 1)]^T$ is the $N_f L_r \times 1$ noise vector that consists of additive white Gaussian noise (AWGN), MUI, and NBI. Notice that the vector $\boldsymbol{y}_u(k)$ in the *discrete-time* equivalent *input-output relationship* (12) contains nothing but the correlator outputs collected from L_r fingers over N_f consecutive frames corresponding to the kth symbol. To decode a symbol, diversity combining needs to be carried out. With the $N_f L_r \times 1$ weight vector $\boldsymbol{\beta}$, diversity combining yields the decision statistics for the kth symbol: $z_u(k) := \boldsymbol{\beta}^T \boldsymbol{y}_u(k)$.

If the noise $\eta(t)$ is white, maximum ratio combining (MRC) is optimal and gives rise to weight vector $\beta_{\text{mf}} := \boldsymbol{c}_u \otimes \tilde{\boldsymbol{\alpha}}$, which implements matched filtering (MF). In the presence of MUI and/or NBI, the noise $\eta(t)$ is often colored, which renders MF weights suboptimal and motivates the use of minimum mean-square error (MMSE) weights: $\boldsymbol{\beta}_{\text{mmse}} := \mathcal{E}_u [\boldsymbol{R}_\eta + \mathcal{E}_u (\boldsymbol{c}_u \otimes \tilde{\alpha})(\boldsymbol{c}_u \otimes \tilde{\alpha})^T]^{-1} (\boldsymbol{c}_u \otimes \tilde{\boldsymbol{\alpha}})$, where $\boldsymbol{R}_\eta := E \times \{\boldsymbol{\eta}(k) \boldsymbol{\eta}^T(k)\}$ is the aggregate noise covariance matrix. It is worth clarifying that the MMSE weights $\boldsymbol{\beta}_{\text{mmse}}$ consists of $N_f L_r$ distinct elements, whereas $\boldsymbol{\beta}_{\text{mf}}$ consists of repetitions of L_r distinct elements. Consequently, MF combining has lower complexity than MMSE combining.

Established based on a two-step (correlation followed by weighted combination) approach, (11) requires *frame-rate* sampling per finger. Interestingly, receiver processing can be implemented even with *symbol rate* sampling. To see this, recall first that the entries of $\boldsymbol{\beta}$ (that is, $[\boldsymbol{\beta}]_n\ \forall n \in [0, N_f L_r - 1]$) are the diversity combining weights. Rake reception that yields the decision statistics $z_u(k)$ can be realized by correlating $r_u(t)$ with the *symbol-long* template $\bar{p}_s(t) = \sum_{n=0}^{N_f - 1} \sum_{l_r=0}^{L_r - 1} [\boldsymbol{\beta}]_{nL_r + l_r}\ p(t - nT_f - \tilde{\tau}_{l_r})$, and sampling its output every $T_s = N_f T_f$ seconds.

To generate the template $\bar{p}_s(t)$, multiple analog waveforms $p(t)$ have to be generated and delayed accordingly. The delay accuracy will affect decoding performance. But different from pulse-rate sampling that requires precise timing at each sampling instance, $\bar{p}_s(t)$ needs to be generated only once during the channel coherence time. The latter provides the timing circuits sufficient time to stabilize and thus reduces timing jitter effects.

Quantifying the UWB Channel's Multipath Diversity

Let us now quantify the order of the multipath diversity collected by a Rake receiver with L_r fingers. To this end, we assume that the channel, which is a realization of the S-V model, is perfectly known at the receiver. We also take the noise to be white, and use the MF weights for MRC. With binary modulation, it is shown in [78] that the average BER is upper bounded as follows:

$$\begin{aligned} \mathrm{P}_e &\leq \prod_{l_r=0}^{L_r-1} \mathrm{E}\left[\exp\left(-\rho\tilde{\alpha}_{l_r}^2/2\right)\right] \\ &= \prod_{l_r=0}^{L_r-1} \left(1+\rho\mathrm{E}\left\{\tilde{\alpha}_{l_r}^2\right\}\right)^{-1/2} \leq \left(A_{L_r}\rho\right)^{-L_r/2}, \end{aligned} \quad (14)$$

where ρ is the transmit signal-to-noise ratio (SNR), A_{L_r} is the geometric average of $\left\{\mathrm{E}\{\tilde{\alpha}_{l_r}^2\}\right\}_{l_r=0}^{L_r-1}$, and the second inequality holds at high SNR ($\rho \gg 1$). Recall that $\left\{\alpha_{l_r}\right\}_{l_r=0}^{L_r-1}$ are the amplitudes of the effective channel taps [c.f. (11)]. Equation (14) confirms that as the number of fingers L_r increases, the diversity order also increases. Also notice that although $N_f L_r$ samples are collected in (13), the diversity order is only $L_r/2$, instead of $N_f L_r/2$, because the degrees of freedom are only $L_r/2$, and the factor 1/2 comes from the fact that the UWB channel is real. The average BER corresponding to binary PAM, and PPM for two values of the modulation index is plotted in Figure 7. As L_r increases, the increase in diversity order is evident.

Two remarks are in order. First, the Rake reception model we presented here is valid when TH is absent. A general Rake reception model along with a unifying signal-to-interference-and-noise ratio (SINR) analysis of low duty-cycle UWB access through multipath and NBI can be found in [82]; see also [11] for a system model based on oversampling. Secondly, even when TH is absent, DS-, SC- and MC-UWB may exhibit different diversity and coding gains when $T_f < \tau_L + T_p$ and IFI emerges. For further details in this direction, readers are referred to [77].

So far, we have outlined how Rake reception can collect diversity, provided that the multipath channel can be estimated at the receiver. Since the received waveform $r_u(t)$ contains many delayed and scaled replicas of the transmitted pulses, a large number of fingers is needed for energy capture. Performing Rake reception with appropriate weights on individual fingers entails estimation of the channel impulse response. This poses a major challenge in UWB communications because even if one opts to utilize only a few (say the ten strongest out of hundreds of) returns, accurate estimation of the ten strongest channel gains and their corresponding delays is required. In a UWB channel with hundreds of multipath returns, channel estimation is oftentimes easier said than done.

Channel Estimation

Although channel estimation is also critical in the context of narrowband and spread-spectrum (SS) systems (see e.g., [63]), and the channel estimators developed for DS-CDMA can be adapted to UWB systems, the formidably high sampling rates required by the latter motivates search for alternatives. The main reason is that the number of parameters to be estimated, i.e., the number of delays and amplitudes, can be as large as 400 for a typical UWB indoor channel.

Impulse response estimators for UWB channels have been developed in [28] and [73] based on the ML criterion. The input-output channel identification algorithm in [73] uses a single transmitted pulse in the absence of MUI; whereas the approaches in [28] form impulse response estimates using either training symbols (data-aided), or unknown information-conveying symbols (nondata-aided), treating MUI as white Gaussian noise. Not surprisingly, [73] arrives at the same channel estimator as the data-aided approach in [28], under the assumption that all multipath components are resolvable, i.e., $|\tau_{l_1} - \tau_{l_2}| > T_p$, $\forall l_1 \neq l_2$. Both data-aided (DA) and nondata-aided (NDA) channel estimators are tested in [28] over a fixed channel with three multipath components, based on 100 symbols. Computational complexity of the ML channel estimators in [28] and [73] increases as the number of multipath components increases, and becomes unaffordable for a realistic UWB indoor channel. Moreover, sampling at subpulse rate is required to perform channel estimation. In [28], the sampling rate of $12.5/T_p \sim 25/T_p$ Hz is suggested. With typical $T_p = 0.7$ ns, the sampling rate is in the formidable

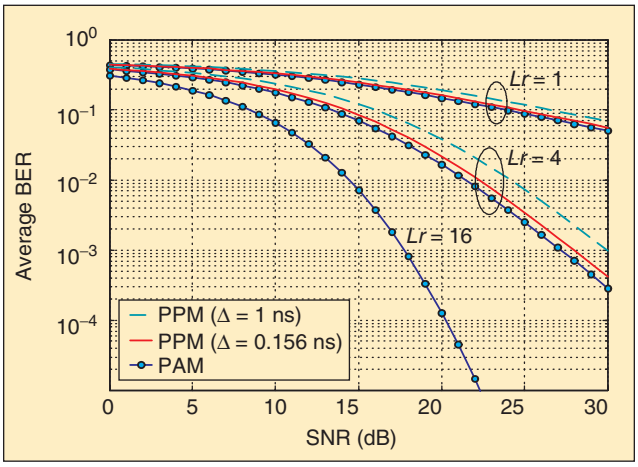

▲ *7. Collecting multipath diversity with Rake reception ($T_p = 0.7$ ns).*

range of 17.9 ∼ 35.7 GHz. At the expense of additional hardware, such rates can only be feasible with staggered sampling using a bank of polyphase ADCs with accurate timing control.

More recently, joint timing synchronization and channel estimation has been pursued. In [6], least squares (LS) estimates of the timing offset τ_0 and the channel impulse response $h(t) = \sum_{l=0}^{L} \alpha_l (t - \tau_l)$ are formed using Nyquist rate (subpulse rate) samples of the received waveform. The clustered structure of the channel is taken into account in forming these estimates. But in addition to oversampling, this approach entails rather restrictive assumptions which include $\tau_0 < T_f$, $\tau_{L,0} < T_f$, knowledge of the channel impulse response structure and order L. Aiming at sub-Nyquist sampling rate, [31] translates the channel impulse response estimation problem into a harmonic retrieval problem. Under the condition $\tau_{L,0} < T_f$ and with the knowledge of L, this method can only form an estimate of a circularly shifted $h(t)$ with the *unknown* $\tau_0 (\text{mod } T_f)$, simply because harmonic retrieval approaches are blind to unknown circular shifts. In other words, [31] cannot estimate timing offsets. To this end, the FFT based approach in [68] combined with a separate timing estimator offers a viable alternative for offline UWB channel estimation at least for PPM transmissions (similar to [6], [28], and [73]), high sampling requirements prevent online implementation of [68].

Transmitted Reference and PWAM Signaling

To avoid the high sampling rate and computational complexity associated with the estimation of $h(t)$, an alternative approach is to estimate the aggregate analog channel $g(t) = (p \star h)(t)$. To this end, there has been a renewed interest in the so termed TR signaling [54], whose application to UWB systems was proposed in [57] for radar detection, and in [21] for communications. In TR systems, each information-conveying pulse is coupled with an unmodulated (a.k.a. pilot) pulse; e.g., per PAM symbol $s = \{\pm 1\}$, we transmit $v(t) = p(t) + s \cdot p(t - T_f)$. After multipath propagation, the received waveform is given by $r(t) = g(t) + s \cdot g(t - T_f) + \eta(t)$. With frame duration chosen to be $T_f \geq \tau_L + T_p$, the received pilot and information conveying waveforms are nonoverlapping. The receiver then correlates $r(t)$ with its delayed version $r(t - T_f)$, to yield the symbol estimate [21]:

$$\hat{s} = \text{sign}\left\{ \int r(t) r(t - T_f)\, dt \right\}, \qquad (15)$$

which, in the absence of noise, yields $\hat{s} = \text{sign}\{s \int g^2(t) dt\} = s$.

Equation (15) is reminiscent of the TDT estimator in (8). However, there are fundamental differences between the TR approach for channel estimation and symbol demodulation and the TDT synchronizer. The first main difference is that TR assumes that noisy templates are taken at the correct time instances; i.e., τ_0 is known and corrected by $\tau = \tau_0$; whereas templates in TDT are not only noisy and distorted by the unknown channel, but also subject to the *unknown* τ_0. Of course, the second major difference is that TDT does not incur the 50% rate/energy loss of TR, where half of transmitted waveforms are used as pilots, regardless of the channel.

To optimize the emerging channel estimation performance-rate tradeoff, a so-called pilot waveform assisted modulation (PWAM) for UWB systems was developed in [81]. As depicted in Figure 8, pilot (a.k.a. training) pulses are inserted in PWAM, and an estimate of the aggregate analog channel $g(t)$ is formed at the receiver by simply averaging over several received pilot waveforms (see also Figure 9). This estimate $\hat{g}(t)$ can then be used as a correlator template, to enable integrate-and-dump demodulation at frame rate (10 MHz with a typical $T_f = 100$ ns).

Clearly, TR is a special case of PWAM where a pilot pulse is inserted after every information pulse. Since the correlator relies on a "noisy template," one expects the error performance at the PWAM detector output to be similar to that of differential decoding. In the latter, each information symbol is detected by using a received symbol as a "noisy pilot" to eliminate the unknown channel gain from the subsequent received symbol.

Key parameters of PWAM include the number of pilot pulses inserted per burst and the energy allocation among pilot and information-conveying pulses. These parameters determine not only the channel estimation

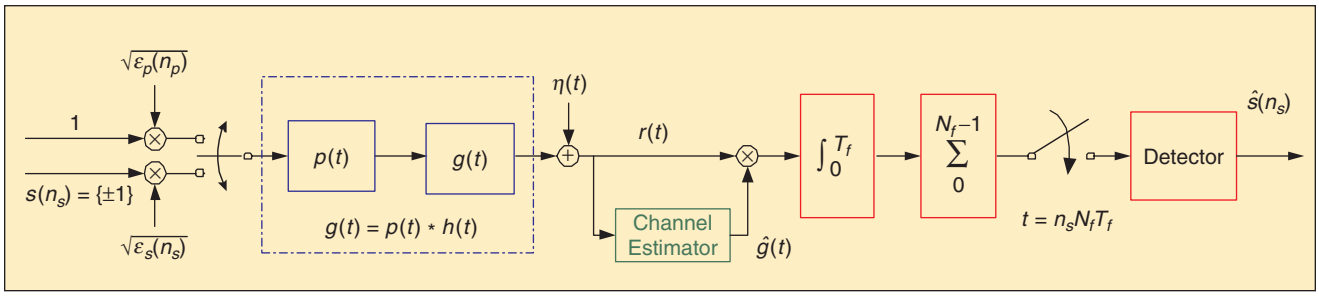

▲ *8. PWAM system block diagram. $\mathcal{E}_s(n_s)$ and $\mathcal{E}_p(n_p)$ denote the energy of information-conveying and pilot waveforms, respectively; $\eta(t)$ is the additive noise; $r(t)$ stands for the received waveform; and $\hat{h}(t)$ represents the estimate of $h(t)$.*

and symbol demodulation performance but also the effective data rate. In fact, optimal parameters can be selected to not only minimize the mean-square channel estimation error and achieve the CRB but also maximize the average capacity [81]. For any given N_f, T_f, and number of waveforms per burst $N = \lfloor \tau_c / T_f \rfloor$ that is determined by the channel coherence time τ_c, the optimal number of pilot waveforms is given by $N_p = N - N_f(\lceil N/N_f \rceil - 1)$ [81]. A fraction α of the total energy per burst is assigned to pilot waveforms, with $\alpha = 0.5$ at low SNR or small N, and $\alpha = \sqrt{N_f}/(\sqrt{N - N_p} + \sqrt{N_f})$ at high SNR or large N. Moreover, equispaced, equipowered pilot waveforms maximize the average capacity as well as provide robustness to slow channel variations. In addition, allocating the number of pilot pulses according to channel coherence time, the flexibility inherent in PWAM allows it to span the gamut of power-limited to bandwidth-limited scenarios [81].

Figure 10(a) depicts the average capacity corresponding to optimal (equi-SNR) PWAM, TR, and the case of perfect channel estimate, with BPSK modulation. The gap is evident, and is increasing as SNR increases. Notice that after 10 dB, the average capacity corresponding to PWAM approaches one, whereas that corresponding to TR approaches 0.5 due to its inherent 50% rate loss. With channel coherence time $\tau_c = 0.2$ ms, and $T_f = 100$ ns, the burst size is $N = 2000$, the average BER versus SNR ρ is plotted in Figure 10(b) for both optimal PWAM and ideal channel estimate. Random TH code is used, and the MUI is modeled as Gaussian noise [72]. When multiple users are present, degradation in BER performance can be observed both with PWAM and with a perfect channel estimate.

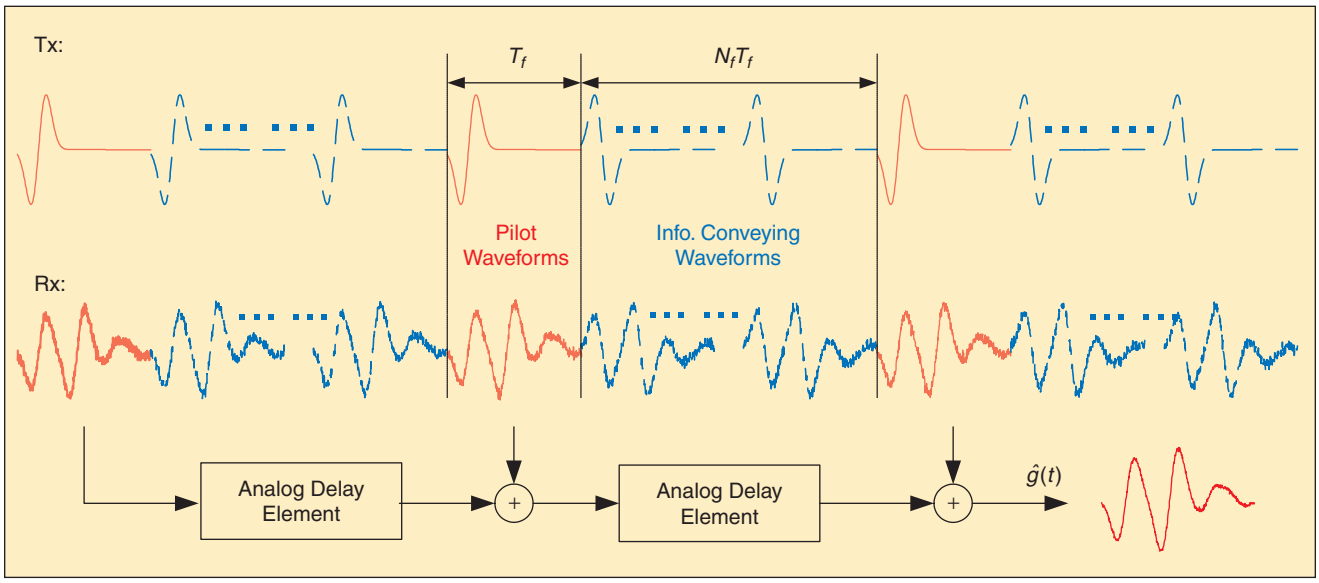

▲ *9. Channel estimation with PWAM ($N = \lfloor \tau_c / T_f \rfloor = 3N_f + 3$, $\bar{N}_p = 3$).*

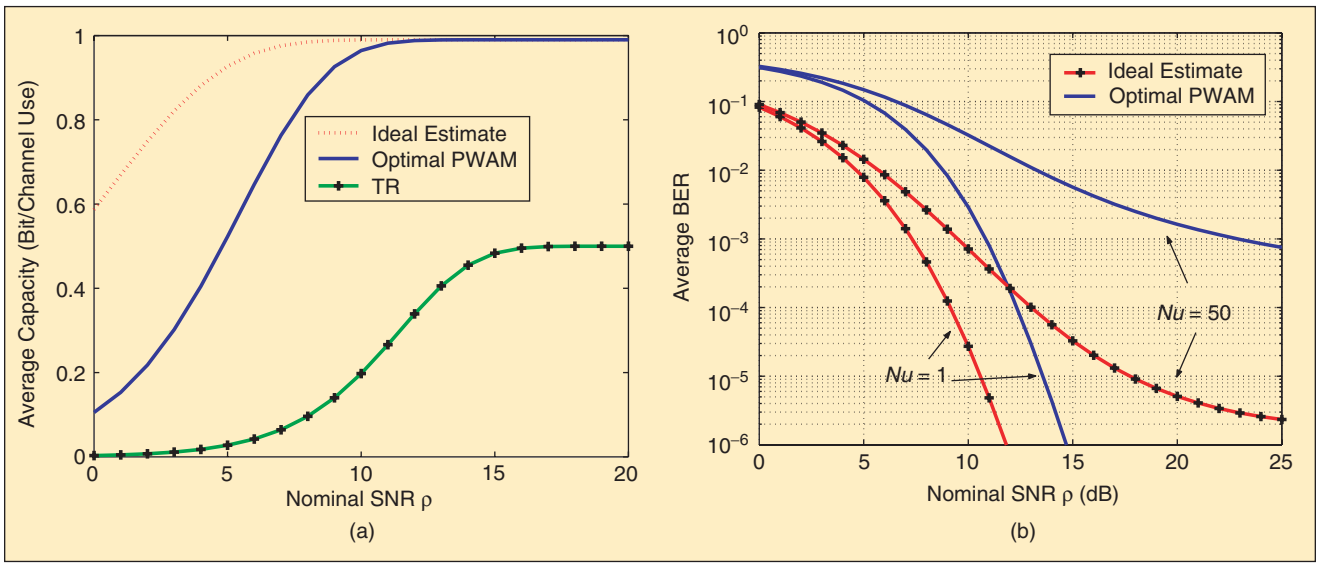

▲ *10. (a) Average capacity versus SNR and (b) BER performance in the presence of MUI.*

Aiming at training-based channel estimation, PWAM is reminiscent of the pilot symbol assisted modulation (PSAM), which was originally developed for bandlimited time-selective channels, and has recently been extended to narrowband frequency-selective channels [36]. Nevertheless, they differ in several aspects: i) PSAM applies to narrowband channels with ISI, whereas PWAM estimates UWB channels that entail no ISI; ii) PSAM estimates the taps of discrete-time equivalent frequency-selective channels, whereas PWAM recovers the equivalent continuous-time channel waveform; and iii) corresponding to one pilot symbol used in PSAM, PWAM allocates multiple pilot pulses across frames and is thus more flexible to strike desirable rate-performance tradeoffs arising with variable channel coherence time.

Although TR was originally advocated for its low-complexity, there has been a number of recent TR improvements that trade off complexity for performance. In the context of delay-hopped (DH-)TR, [84] proposes an ML receiver whose implementation requires the autocorrelation of the physical channel $h(t)$ at various delays, and calls for a systematic signal design methodology. In TR and PWAM, the continuous-time aggregate channel is estimated from the pilot waveforms only. Further exploiting the channel information embedded in the information-conveying waveforms, ML and generalized likelihood ratio tests (GLRTs) schemes were put forth in [7]. Trading off complexity for performance, [7] turns out to be a channel impulse response estimator with high complexity as the ones in [28] and [73].

Differential and Noncoherent UWB

As both timing synchronization and channel estimation pose major challenges in UWB communications, *noncoherent* UWB radios that bypass both of these challenging tasks offer interesting alternatives to explore.

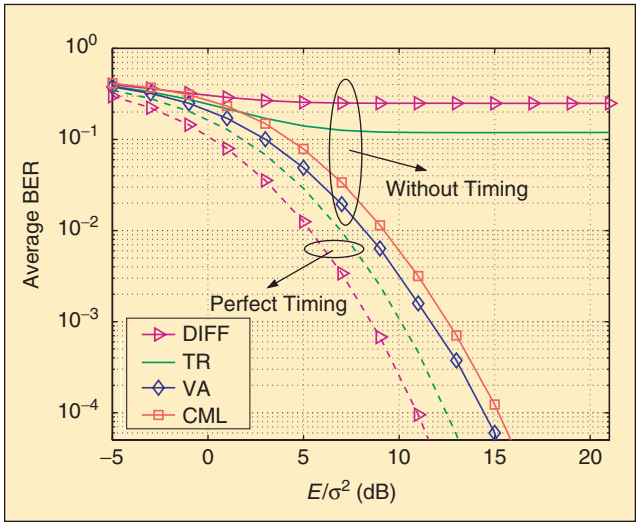

▲ *11. Performance of TR and differential (DIFF) UWB in the presence and absence of timing offsets; and that of incoherent UWB radios using VA and CML demodulators in the presence of timing offsets.*

Consider a single-user link with binary PAM with DS/SC/MC and/or TH spreading codes. Moreover, let us differentially encode the binary PAM (BPSK) symbols $a(k)$ as $\tilde{a}(k) := a(k) \cdot \tilde{a}(k-1)$ and transmit the encoded sequence $\tilde{a}(k)$. The received waveform is then given by [c.f. (5)]:

$$r(t) = \sqrt{\mathcal{E}} \sum_{k=0}^{\infty} \tilde{a}(k) p_R(t - kT_s - \tau_0) + \eta(t),$$

where the timing offset $\tau_0 \neq 0$ in general. Performing the integrate-and-dump operations using dirty templates as in (6), the symbol-rate samples are [c.f. (7)]

$$\begin{aligned} x_k &= \int_0^{T_s} r(t + kT_s) r(t + (k+1)T_s)\, dt \\ &= a(k)\mathcal{E}_A(\tau_0) + a(k+1)\mathcal{E}_B(\tau_0) + \xi(k), \end{aligned} \quad (16)$$

where we used the fact that $a(k) = \tilde{a}(k)\tilde{a}(k-1)$ in establishing the second equality.

If one opts to estimate the timing offset using, e.g., the TDT approach, and compensate it (almost) perfectly, then (16) can be considered approximately with $\tau_0 = 0$. In this case, $\mathcal{E}_A(0) = 0$, $\mathcal{E}_B(0) = \mathcal{E}_R$ and (16) boils down to $x_k = a(k+1)\mathcal{E}_R + \xi(k)$, which can be easily demodulated. In fact, (16) with $\tau_0 = 0$ shows that the differential UWB system in [7] and [19] can be viewed as a special case of the noncoherent approach. This differential UWB receiver is semicoherent since it requires timing but bypasses channel estimation. The performance of such a differential (DIFF) scheme is shown in Figure 11. It is worth stressing that with perfect timing and for the same information rate, differential UWB outperforms TR simply because the latter uses 50% energy on pilots, as confirmed in Figure 11.

But even when synchronization is attempted, timing errors are inevitable and thus $\tau_0 \neq 0$. In this case, $\mathcal{E}_A(\tau_0)$ and $\mathcal{E}_B(\tau_0)$ are also nonzero and direct application of differential demodulation will lead to considerable performance degradation. Simulated performance of DIFF-UWB and TR in the presence of timing offset is shown in Figure 11. Notice that though TR is more robust against timing offsets than DIFF-UWB, both yield unacceptable performance. However, we observe that the channel energies $\mathcal{E}_A(\tau_0)$ and $\mathcal{E}_B(\tau_0)$ in (16) can be viewed as the impulse response taps of an unknown first-order equivalent ISI channel [83]. This interesting viewpoint motivates development of noncoherent algorithms for joint symbol detection and estimation of the unknown equivalent channel based on the "dirty correlator" output samples in (16). It is worth stressing that only two equivalent channel taps are to be estimated with noncoherent UWB, as apposed to hundreds of taps in the underlying UWB physical channel and the analog aggregate channel in TR and PWAM. Several

noncoherent schemes have been recently considered in [83]. One approach is the ML sequence demodulator using Viterbi's algorithm (VA) along with its low-complexity per-survivor variants. Further trading off performance for complexity, decision-directed conditional ML (CML) alternatives are also explored in [83]. The performance of noncoherent UWB using VA and CML schemes is depicted in Figure 11. Bypassing both timing synchronization and channel estimation, these noncoherent algorithms exhibit as little as 3 dB loss in comparison with differential UWB with perfect timing.

Multi-Antenna UWB Systems

We have seen how the error performance of UWB radios can be boosted by collecting multipath diversity [8], [21], [81]. However, Rake reception in UWB may require a large number of finger amplitudes and delays which are cumbersome to obtain [28], [73]. Avoiding estimation of the channel's impulse response, PWAM and TR require an analog delay line at the receiver which may not be easy to implement [13]. Differential and noncoherent schemes enjoy low complexity at the price of suboptimum performance. In a nutshell, although rich multipath diversity is enabled with UWB transmissions, its collection at the receiver may face implementation difficulties, especially when the channel variations are relatively rapid.

On the other hand, multi-antenna-based space-time (ST) systems offer an effective means of enabling space diversity via spatial multiplexing, which has the potential to improve not only error performance, but also capacity. Motivated by these attractive features, an *analog* ST coding scheme was developed for UWB communications in [78]. With the channel coherence time being at least one symbol duration $\tau_c \geq T_s = N_f T_f$, the following ST coded matrix is transmitted:

$$\sum_{n=0}^{N_f/2-1} \begin{bmatrix} v_u^{00}(n;t) & v_u^{01}(n;t) \\ v_u^{10}(n;t) & v_u^{11}(n;t) \end{bmatrix}, \quad \forall t \in [0, T_s) \qquad (17)$$

where $v_u^{kl}(n;t)$ denotes the waveform transmitted from the kth transmit antenna during the $(2n+l)$th frame duration. The matrix entries in (17) can be expressed explicitly as

$$\begin{aligned} v_u^{00}(n;t) &= a_u(2n)c_u(2n)p\big(t-2nT_f \\ &\quad -c_u^{TH}(2n)T_c - b_u(2n)\Delta\big) \\ v_u^{01}(n;t) &= a_u(2n)c_u(2n+1)p\big(t-(2n+1)T_f \\ &\quad -c_u^{TH}(2n+1)T_c - b_u(2n)\Delta\big) \end{aligned}$$

$$\begin{aligned} v_u^{10}(n;t) &= a_u(2n)c_u(2n+1)p\big(t-2nT_f \\ &\quad -c_u^{TH}(2n)T_c - b_u(2n)\Delta\big) \\ v_u^{11}(n;t) &= -a_u(2n)c_u(2n)p\big(t-(2n+1)T_f \\ &\quad -c_u^{TH}(2n+1)T_c - b_u(2n)\Delta\big), \end{aligned}$$

where we used the fact that $a_u(2n+1) = a_u(2n)$, and $b_u(2n+1) = b_u(2n)$, $\forall n \in [0, N_f/2-1]$. This UWB-specific scheme is different from existing ST codes used for digital linear modulations [3] in three aspects.

▲ i) *Digital symbol-by-symbol versus analog within each symbol waveform*. Existing STC schemes operate on digital symbols, whereas this UWB-tailored STC approach encodes pulses within symbol waveforms; it is this UWB-specific aspect that enables enhanced space-multipath diversity gains;

▲ ii) *Flat or ISI-inducing channels versus frequency-selective channels*: Existing STC schemes are designed either for flat, or, for ISI-inducing MIMO fading channels, whereas this analog ST code is tailored for non-ISI inducing UWB MIMO channels that are rich in multipath diversity;

▲ iii) *Linear and nonorthogonal nonlinear modulations versus linear and orthogonal nonlinear modulations with coherent or noncoherent reception*. Existing STC schemes entail linear modulators and coherent demodulators, except for the works of [20] that deal with the noncoherent case. However, the latter do not consider orthogonal nonlinear modulations (orthogonal PPM) that are of interest to UWB and lead to ST coding schemes that guarantee full diversity and symbol detectability, even with noncoherent reception.

With one receive and two transmit antennas and PAM modulation in the absence of TH, it can be shown that the average BER for binary modulations at high receive-SNR ρ is upper bounded by [78]:

$$\mathrm{P}_e \leq \left(\frac{A_{L_r}}{2}\rho\right)^{-L_r}, \qquad (18)$$

where L_r is the number of Rake fingers, and A_{L_r} is the geometric average of $\{\mathrm{E}\{\tilde{\alpha}_{l_r}^2\}\}_{l_r=0}^{L_r-1}$. Compared with (14), this ST coded transmission scheme doubles the diversity order, but loses 3 dB coding gain, due to the power split between the two antennas at the transmitter. In an indoor environment with low mobility, the channel coherence time τ_c is generally much larger than the frame duration T_f. This suggests employment of an interleaver in conjunction with ST coding. With the multipath channel remaining invariant over one symbol duration $T_s = N_f T_f$, and changing independently from symbol to symbol, it is shown in [78] that using an interleaver with depth $N_d \leq N_f$ yields an average BER upper bounded as follows:

$$\mathrm{P}_e \leq \left(\frac{A_{L_r}}{2N_d}\rho\right)^{-N_d L_r}. \qquad (19)$$

Achieving diversity N_d times that in (18) with the same L_r and identical channel estimation complexity, the price paid is decoding delay by N_d symbols and loss in coding gain by a factor N_d.

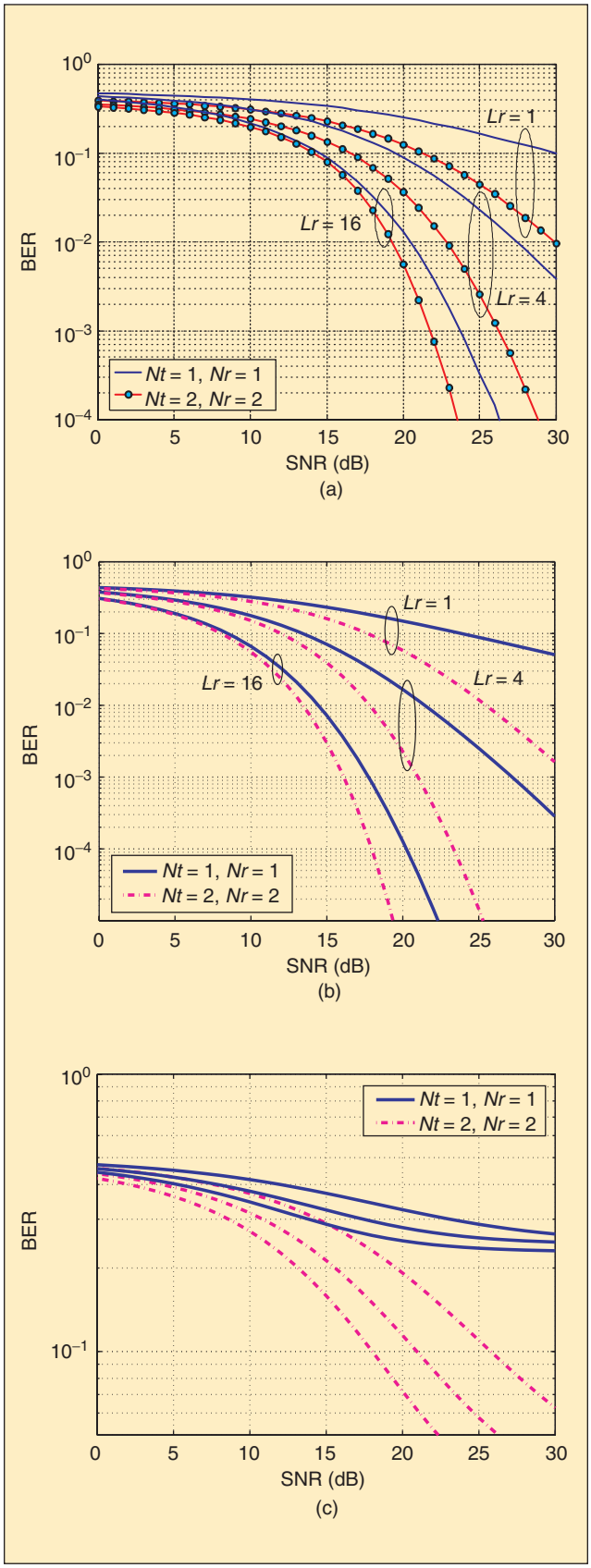

▲ *12. (a) Incoherent reception; (b) coherent reception in the absence of timing jitter; (c) coherent reception in the presence of timing jitter (from top to bottom $L_r = (1, 4, 16)$). Timing jitter is modeled as exponentially distributed with mean 0.5 ns; N_t and N_r stand for the number of transmit and receive antennas, respectively.*

While enhancing the diversity gains by deploying an additional antenna, ST-coded multi-antenna UWB radios can be implemented with conventional analog Rake receivers having a small number of fingers. ST-UWB also enables noncoherent reception for joint diversity collection, which bypasses the cumbersome channel estimation task [78]. Figure 12 shows simulated performance of an ST-coded multi-antenna UWB system with coherent and noncoherent reception in the presence of timing jitter. Simulations reveal considerable improvement in both BER, and enhanced immunity against timing jitter. The latter suggests theoretical analysis of its robustness against timing jitter, and the potential of multiple antennas to facilitate synchronization of UWB systems.

Multiple Access and Interference Suppression

In the presence of multiple users and overlaying narrowband systems, single user detection is typically suboptimal, and special effort is needed to cope with MUI and/or NBI effects. This subsection will be devoted to such issues.

Single-Carrier and Multicarrier Codes:

Let us recall the baseband multi-access UWB setup in (3) with the user-specific spreading codes $c_u(n)$ being symbol-periodic with period N_f. We also normalize the spreading codes such that $\sum_{n=0}^{N_f-1} c_u^2(n) = N_f$. In DS-UWB, orthogonal binary sequences $c_u(n) \in \{\pm 1\}$ are employed: $\sum_{n=0}^{N_f-1} c_{u_1}(n)c_{u_2}(n) = N_f\delta(u_1 - u_2)$. Similar to TH-UWB, these codes are constant-modulus and have been used in e.g., [15], [48], [76]. However, utilizing the entire bandwidth, they are not flexible in handling NBI. To this end, digital single-carrier (SC-) and multicarrier (MC-)UWB have been introduced recently, for low-power low-duty-cycle baseband UWB multiple access [77].

Casting the user-specific spreading codes $c_u(n)$ into $N_f \times 1$ vectors $\boldsymbol{c}_u$ with user index $u \in [0, N_u - 1]$, the construction of SC/MC-UWB codes $\boldsymbol{c}_u$ starts with $N_u = N_f$ orthogonal baseband digital subcarriers $\forall k \in [0, N_f - 1]$:

$$[\boldsymbol{f}_k]_n = \begin{cases} \cos\left(\frac{2\pi n}{N_f}k\right), & n = 0, \text{or}, n = N_f/2, \\ \sqrt{2}\cos\left(\frac{2\pi n}{N_f}k\right), & n \in [1, N_f/2 - 1], \\ \sqrt{2}\sin\left(\frac{\pi(2n-N_f)}{N_f}k\right), & n \in [N_f/2 + 1, N_f - 1], \end{cases}$$

where $[\boldsymbol{f}_k]_n$ denotes the $(n+1)$ st entry of the column vector $\boldsymbol{f}_k$. The discrete-time Fourier transform (DTFT) of $\boldsymbol{f}_k$ contains sinc functions, as depicted in Figure 13(a). Now let $\{\boldsymbol{c}_u^{(o)}\}_{u=0}^{N_f-1}$ denote any set of orthonormal spreading codes of length N_f. User-specific codes for baseband MC-UWB can then be constructed as linear combinations of digital subcarriers

$$\boldsymbol{c}_u = \sum_{k=0}^{N_f-1} \left[\boldsymbol{c}_u^{(o)}\right]_k \boldsymbol{f}_k. \qquad (20)$$

Notice that baseband SC-UWB is subsumed by (20), if one selects $\{\boldsymbol{c}_u^{(o)}\}_{u=0}^{N_f-1}$ as distinct columns of a $N_f \times N_f$ identity matrix. (For each user (subcarrier) to occupy exactly the same bandwidth, a $0.5/N_f$ shift has to be introduced to the digital subcarriers as detailed in [77].) Different from orthogonal frequency division multiple access (OFDMA) in narrowband systems [67], the baseband SC/MC codes in (20) are real. Spreading every symbol on a *single* digital subcarrier, each SC-UWB user occupies $2T_f/T_p \gg 2$ frequency bands (see Figure 13), and the resulting transmissions enjoy multipath diversity gains; whereas narrowband OFDMA systems have to resort to channel coding and/or frequency hopping to mitigate frequency-selective fading at the expense of (possibly considerable) bandwidth overexpansion.

In [77], the performance of DS-, SC- and MC-UWB is quantified in terms of diversity and coding gains, when IFI is present but ISI is avoided by zero-padding or cyclic-prefixing. Analysis shows that SC/MC codes enable full multipath diversity gain, and MC codes can further effect maximum coding gain. Additionally, SC- and MC-UWB codes offer flexibility in handling (e.g., WLAN induced) NBI, simply by avoiding the corresponding digital subcarriers. The same flexibility in avoiding NBI is also present in the spectrally encoded (SE-) UWB system of [9]. With SC/MC codes, the ultrawide bandwidth is partitioned into segments, each corresponding to a digital carrier. Likewise, SE-UWB also partitions the bandwidth into a number of frequency bands (so-called frequency "chips"). A sequence of codes (much as $\boldsymbol{c}_u^{(o)}$ in (20) for SC/MC-UWB) can then be applied on these "chips" to enable MA. As a result, both SC/MC- and SE-UWB can avoid NBI affected frequency segments—digital carriers in SC/MC-UWB and frequency "chips" in SE-UWB—by nulling the corresponding elements of the code vector $\boldsymbol{c}_u^{(o)}$. Constructed based on digital cos/sin functions, SC/MC-UWB facilitates low-complexity implementation using standard discrete-cosine-transform (DCT) circuits. (This implementation advantage also distinguishes them from the analog SC-UWB codes introduced in [66] that offer robustness against user asynchronism.) SE-UWB, on the other hand, can be implemented using surface acoustic wave (SAW) devices [9]. As SC/MC-UWB, the resultant SE-UWB also enables multipath diversity by sweeping the ultra-wide bandwidth within pulse duration T_p, much as in fast frequency hopping (FH) systems.

Performance comparisons among DS, SC, and MC spreading codes, individually or in combination with TH codes, have been carried out when NBI is present, under a general SINR analysis framework that allows for various Rake finger selections [82]. Several

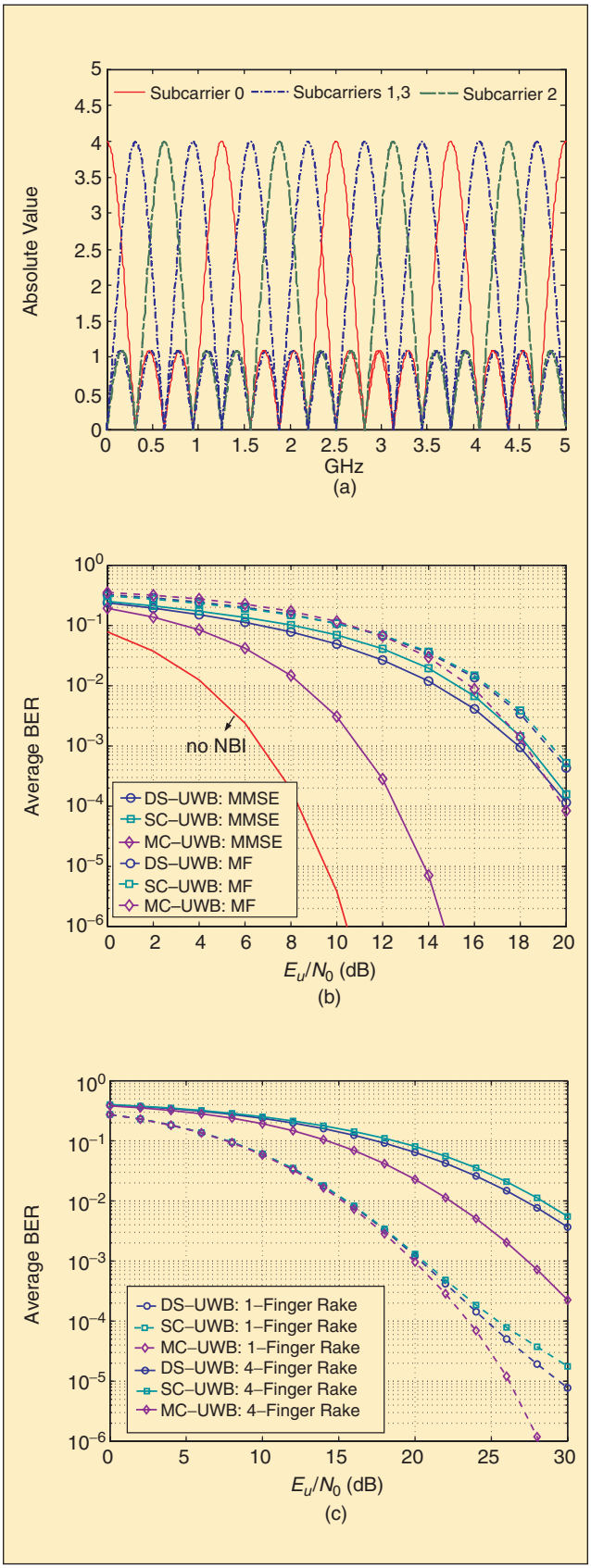

▲ *13. (a) Subcarriers in baseband SC- and MC-UWB ($N_f = 4$, $T_f/T_p = 4$, $T_p \approx 0.2$ ns). Average BER corresponding to DS-, SC-, and MC-UWB over AWGN with NBI at the GPS band (center frequency 1.2 GHz, bandwidth 20 MHz) in (b) AWGN channel; (c) multipath channel (selective-Rake with MMSE combining).*

interesting conclusions can be drawn from these comparisons. In particular, analytical and simulated results show that MC-UWB provides code-independent BER performance in the presence of multipath and NBI effects, regardless of the Rake finger selection. The BER averaged over all codes is shown in Figure 13(b) for AWGN channels and in Figure 13(c) for multipath channels, both in the presence of NBI. From these comparisons, baseband MC-UWB emerges as an attractive choice for antijam applications without nulling any subcarriers. This avoids additional processing for collision detection or clear channel assessment (CCA), and ensures small size transceivers with low power consumption.

Different from the WPAN multiband proposals that rely on analog carriers (see, e.g., [4]), the SC/MC codes achieve multiband transmission using baseband operations. Compared to analog multiband solutions that entail multiple local oscillators, carrier-free multiband SC/MC-UWB access not only enjoys low-complexity implementation but also avoids dealing with carrier frequency offsets that are known to degrade error performance (of e.g., OFDMA) severely.

The schemes we have discussed so far for UWB multiple access are either constant modulus or provide robustness and flexibility against NBI. But with DS/SC/MC spreading codes, perfect multi-user separation with $N_u = N_f$ users is possible only if $T_f \geq \tau_L + T_p$, that is, when rate considerations allow one to select a frame duration which is longer than the maximum delay spread augmented by one pulse duration. When TH spreading codes are employed, or when $T_f < \tau_L + T_p$ is chosen to achieve high data rates, the mutual orthogonality among users' spreading codes is destroyed after multipath propagation [15], [25]. This introduces MUI, which compromises capacity and error performance considerably [25], unless complex receiver algorithms are employed to mitigate it.

Conventionally, MUI is treated as Gaussian noise, and is suppressed statistically with the aid of (strict) power control [72]. However, when the number of users is not large enough, the Gaussian approximation of MUI is not valid, especially with imperfect power control [10], [16].

MUD for UWB Access

To improve upon the statistical MUI cancellation, UWB-MA utilizing multi-user detection (MUD) was pursued in [32]. In fact, [32] established the first digital model for UWB-MA systems, where novel approaches were developed to account for the nonlinear PPM modulation and TH spreading. The digital model triggered the transition from analog UWB to digital UWB, and these novel approaches are used also in recent UWB modeling attempts (see, e.g., [11]). Specifically, the continuous time UWB signal using nonlinear M-ary PPM modulation is viewed as M parallel branches each realizing a shifted version of the pulse stream [32], [42], [76]. In other words, the transmitted signal using PPM and TH codes can be expressed as [c.f. (2)]:

$$v_u(t) = \sqrt{\mathcal{E}_u}\sum_{n=0}^{+\infty} p\big(t - \big(nN_c + c_u^{TH}(n)\big)T_c - b_u(n)\Delta\big) = \sum_{m=0}^{M-1} v_u^{(m)}(t), \tag{21}$$

where $v_u^{(m)}(t) := \sqrt{\mathcal{E}_u}\sum_{n=0}^{+\infty} b_u^{(m)}(n)p_m\big(t - \big(nN_c + c_u^{TH}(n)\big)T_c\big)$ with $b_u^{(m)}(n) := \delta(b_u(n) - m)$, and $p_m(t) := p(t - m\Delta)$, $\forall m \in [0, M-1]$. As to the nonlinear TH codes, the *frame-rate* sequence $c_u^{TH}(n)$ can be uniquely mapped to a *chip-rate* TH sequence $\tilde{c}_u^{TH}(k) := \delta\big(c_u^{TH}(\lfloor k/N_c \rfloor) - (k \mod N_c)\big)$ for the kth chip. When $c_u^{TH}(n)$ has period N_f, it can be verified that $\tilde{c}_u^{TH}(k)$ has period $N_f N_c$. But the chip-rate TH sequence can be viewed as a DS code with $\{0, 1\}$ entries, and thus enables representation of nonlinear TH spreading with an equivalent linear DS spreading. Consequently, we have [c.f. (21)]

$$v_u^{(m)}(t) = \sqrt{\mathcal{E}_u}\sum_{k=0}^{+\infty} v_u^{(m)}(k)p_m(t - kT_c),$$

where $v_u^{(m)}(k) := b_u^{(m)}(\lfloor k/(N_c N_f) \rfloor)\tilde{c}_u^{TH}(k)$ is the symbol sequence after TH spreading. Let $g_u^{(m',m)}(l) := (p_m \star h_u \star p_{m'})(-t)|_{t=lT_c}$ of order L_u be the chip-sampled discrete time equivalent finite impulse response (FIR) channel. Then, the chip-sampled matched filter output of the m'th branch at the receiver is

$$x_{m'}(k) = \sum_{u=0}^{N_u-1}\sum_{m=0}^{M-1}\sum_{l=0}^{L_d}\sqrt{\mathcal{E}_u}g_u^{(m',m)}(l)v_u^{(m)}(k-l) + \eta_{m'}(k), \tag{22}$$

where $\eta_{m'}(k)$ denotes the sampled noise and $L_d := \max_u L_u$. It is shown in [32] and [76] that (22) can also be represented in vector-matrix form by utilizing *block* spreading in lieu of *symbol* spreading. The resultant input-output relationship is

$$\boldsymbol{x}_{m'}(i) = \sum_{u=0}^{N_u-1}\sum_{m=0}^{M-1}\sqrt{\mathcal{E}_u}\Big[\boldsymbol{G}_{u,0}^{(m',m)}\boldsymbol{v}_u^{(m)}(i) + \boldsymbol{G}_{u,1}^{(m',m)}\boldsymbol{v}_u^{(m)}(i-1)\Big] + \boldsymbol{\eta}_{m'}(i). \tag{23}$$

Extracted from a continuous-time UWB transmission with *nonlinear* PPM modulation and TH spreading, the digital model in (23) consists of only linear operations. In addition, its serial form (22) and parallel (vector-matrix) form (23) both capture MUI and ISI [manifested

as interblock interference (IBI) in (23)] after multipath propagation. As a result, this digital model allows direct adaptation of narrowband MUD to UWB systems. A number of works have followed this approach. Recursive MUD schemes are also pursued for DS-UWB systems, without assuming channel knowledge at the receiver [27]. It has been illustrated by simulations that such recursive MUD receivers outperform Rake receivers with finite fingers in suppressing both MUI and NBI. However, MUD-based schemes entail sampling at subpulse rate of up to 16 GHz, they require an initializing training sequence of 500 symbols, and rely on decision directed operation that is prone to error propagation. To ensure convergence, the channels for all users must also remain invariant for a sufficiently long period (500 symbols) [27].

Multistage Block-Spread (MSBS) UWB Access

With chip duration $T_c \approx T_p$ and symbol duration $T_s = N_f N_c T_c$, the bandwidth expansion factor in a typical UWB system is $N_f N_c$. But the maximum number of users is $N_u = N_c$ with orthogonal TH, and $N_u = N_f$ with orthogonal DS/MC/SC, both of which have lower user capacity than that allowed by the bandwidth expansion factor. There is certainly space for improvement in terms of multi-user capacity. To this end, a promising so termed multistage block-spread (MSBS) design of spreading codes has been developed [76]. With MSBS-UWB, the number of users that can be accommodated is $N_u = N_f N_c$ by employing DS/SC/MC codes in combination with TH codes. More important, MSBS-UWB provides MUI-resilient performance, even after (possibly unknown) multipath propagation. Relying on two stages of block-spreading and interleaving, the mutual orthogonality among users' spreading codes is guaranteed even after propagation through frequency-selective multipath channels. Consequently, only the desired user's spreading codes are required at the receiver, and a single-user detector is sufficient. As a result, deterministic MUI-resilient reception with low-complexity code-matched filtering becomes possible without loss of ML optimality, and with full multipath diversity gains [76]. Figure 14 compares the BER of MSBS-UWB with conventional TH-UWB using a Rake receiver [52], and with the MUD-UWB receiver [32], over two channel models [25], [50], [76]. In contrast to conventional TH-UWB, MSBS-UWB shows no degradation as the number of users increases. With much lower complexity and many more active users, it also outperforms the MUD-UWB multiple access system.

Single-Band or Carrier-Modulated Multiband?

So far, we have focused on baseband UWB signaling, which occupies a single UWB spectrum from near DC up to a few GHz. Such carrier-free transmissions require minimal RF components. But since UWB radios occupy extremely broad bandwidth, they inevitably overlay existing narrowband RF services, such as GPS, federal aviation systems (FAS), and WLAN. To regulate coexistence, the FCC has released a spectral mask in its first UWB R&O that limits the equivalent isotropic radiated power (EIRP) spectrum density with which UWB radios are allowed to transmit. To realize the attractive features of UWB radios under this FCC regulation, the following challenges have to be addressed:

▲ i) Operating below the noise floor, UWB radios must emit at low power. But as any other communication system, the performance of a UWB system heavily relies on the received SNR that is proportional to the transmit power. Maximization of the latter, however, can be achieved only if the spectral shape of the FCC mask is exploited in a power-efficient manner.

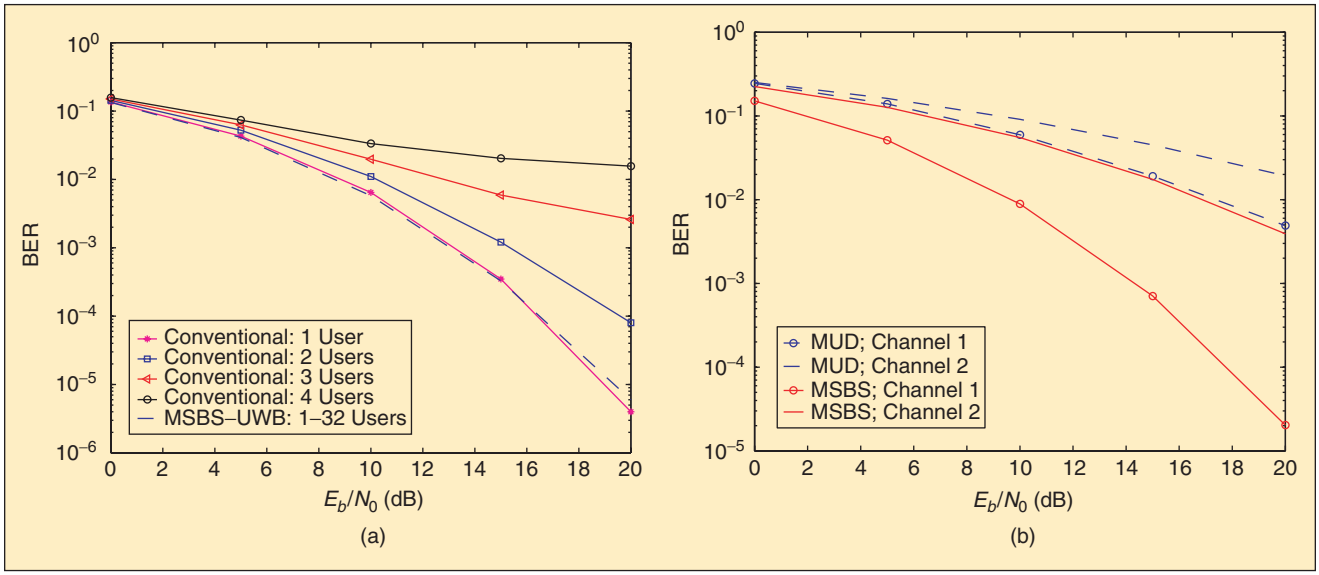

▲ *14. (a) BER comparison of a conventional UWB-MA system with a MSBS-UWB system; (b) BER versus SNR for zero-forcing (ZF) receiver with $N_f = 8$, $N_c = 4$. Number of active users: four in MUD-UWB system, 32 in MSBS-UWB system.*

▲ ii) To avoid interference to (and from) coexisting narrowband systems, their corresponding frequency bands must be avoided. Since the nature and number of coexisting services may change depending on the band used, the avoidance mechanism should also be sufficiently flexible.
▲ iii) Traditionally, UWB multiple access is achieved by employing TH codes. User capacity of UWB radios can be further improved by partitioning the ultra-wide bandwidth into subbands, allowing users to hop among these subbands according to user-specific hopping patterns. Since hopping should span subbands centered around different frequencies, UWB pulse shapers must be agile with respect to FH to enhance system capacity and reinforce the low probability of interception and detection (LPI/LPD).

All these requirements heavily rely on a basic transmitter module—the pulse shaper. Unfortunately, the widely adopted Gaussian monocycle is not flexible enough to meet these challenges [74]. To design pulse shapers with desirable spectral properties, two approaches can be employed: carrier-modulation and/or baseband analog/digital filtering of the baseband pulse shaper. The former relies on local oscillators at the UWB transmitter and receiver, which being prone to mismatch give rise to carrier frequency offset/jitter (CFO/CFJ). In multiband UWB systems with FH, multiple CFO/CFJ emerge with this approach. Although passing the (Gaussian) pulse through a baseband analog filter can reshape the pulse without introducing CFO/CFJ, it is well known that analog filters are not as flexible when compared to digital filters, which are accurate and perfectly repeatable.

Optimal UWB Pulse Shapers

Pulse shapers respecting the FCC mask have been proposed in [40] and [29]. Targeting multiple orthogonal pulses that are FCC mask compliant, [40] developed pulses in digital form that correspond to the dominant eigenvectors of a matrix, which is constructed by sampling the FCC mask. The resulting pulses *meet* the FCC mask, but do not *optimally exploit* the allowable bandwidth and power [see Figure 15(a)]. Unfortunately, converting the digital designs in [40] into analog form entails digital-to-analog (D/A) operations at 64 GHz rate. Imposing minimum modification to the analog components of existing UWB transmitters and aiming at pulses that not only meet, but also optimally exploit the FCC mask, [29] introduced optimal pulse shapers for UWB using the "workhorse" of digital filter design methods, namely the Parks-McClellan algorithm [39]. This idea is to start with *any* continuous-time spectral shaping waveform $p_a(t)$, including the Gaussian monocycle, and design the pulse shaper as

$$p(t) := \sum_{m=0}^{M-1} w_m p_a(t - mT_0), \qquad (24)$$

where w_m are tap coefficients with spacing T_0. Evidently, the choice of T_0 affects w_m, and thus the feasibility, optimality and complexity of the overall design. It is shown in [29] that $T_0 = 35.7$ ps is suitable for optimal designs with full-band control, and $T_0 = 73$ ps for suboptimal designs that trade off performance for complexity. For any T_0 value and $p_a(t)$ with FT $P_a(f)$, [29] casts the pulse shaper design problem boils down to a digital filter design problem, where an M-tap FIR filter with coefficients $\{w_m\}_{m=0}^{M-1}$ is to be designed such that its DTFT magnitude $|W(e^{j2\pi F})|$ approximates $D(F/T_0)$, $\forall F \in [0, 0.5]$, where $D(f) := P_d(f)/|P_a(f)|$, $\forall f \in [0, 0.5/T_0]$ and $P_d(f)$ can be chosen to

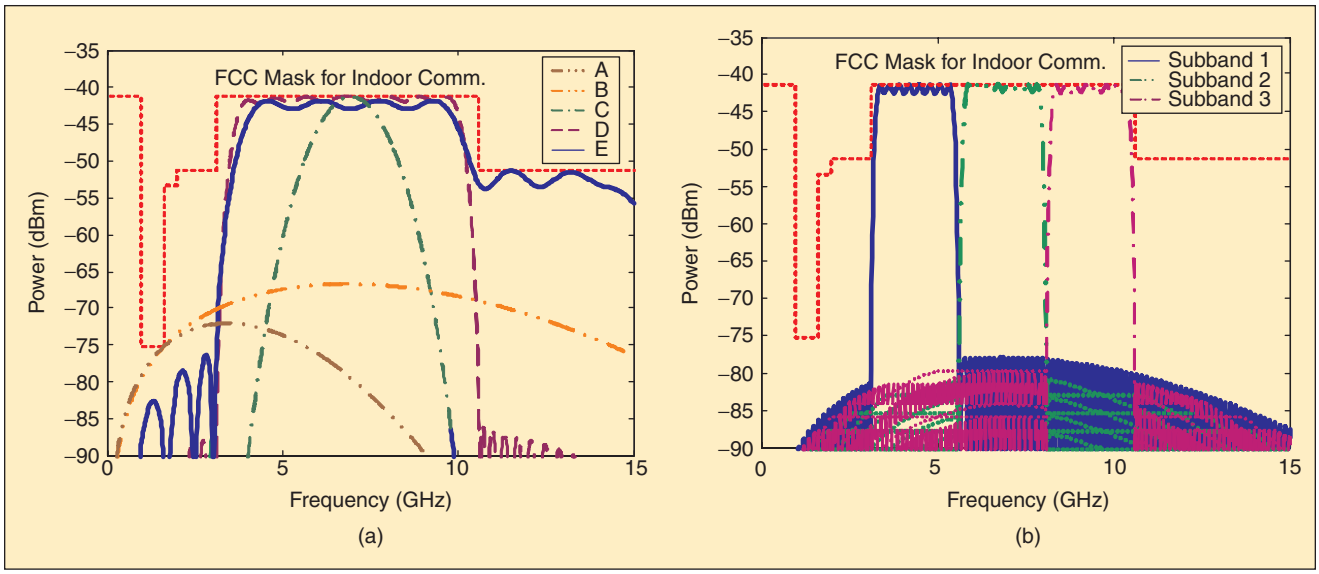

▲ *15. (a) Baseband pulse shapers and the FCC mask for indoor communications. A—Gaussian monocycle with $T_p = 0.37$ ns; B—Gaussian monocycle with $T_p = 0.19$ ns; C—a pulse shaper in [98]; D&E—pulse shapers in [99]; (b) Multiband UWB using baseband pulse shapers.*

satisfy *any* desirable spectral mask specification. Instead of casting the UWB pulse shaper design as a filter design problem, it is also possible to view it as a semi-definite programming (SDP) optimization problem; see [75] for SDP related designs.

Pulse shapers designed according to (24) exploit the FCC spectral mask optimally, and offer flexibility for (dynamic) avoidance of NBI. Comparing three pulse shaper designs in Figure 15(a), it follows that, in order for a Gaussian monocycle $p_a(t)$ to adhere to the FCC mask, it must transmit at $\mathcal{E}_u \leq 0.506\ T_s\mu$J when $T_p = 0.37$ ns, and at $\mathcal{E}_u \leq 3.43\ T_s\mu$J when $T_p = 0.19$ ns; pulse shaper C can transmit at $\mathcal{E}_u \leq 0.25\ T_s$mJ, while pulse shapers D and E can transmit at $\mathcal{E}_u \leq 0.88 T_s$mJ, and $\mathcal{E}_u \leq 0.91 T_s$mJ, respectively [29]. This shows that the optimal designs in [29] can offer 2–3 orders of magnitude more power-efficient pulse shapers. Furthermore, they are well suited for digital implementation of subband hopping (or FH) codes, which are used with *multiband* UWB systems. The latter have gained popularity recently, because they can replace the traditional TH codes for MA, or complement them to enhance capacity and covertness [see Figure 15(b)].

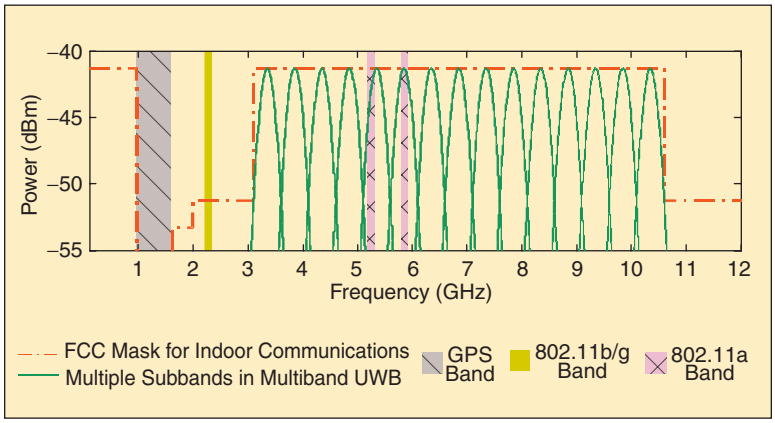

▲ *16. Multiple subbands in multiband UWB.*

Multiband UWB Access

Baseband pulses can also be modulated onto carrier(s) to higher frequency band(s). Recently, there has been an increasing interest in transmissions with multiple subbands, which we henceforth term *multiband* UWB (see e.g., [1], [4], [47]). In multiband UWB radios, pulses are modulated by several analog carriers to subbands 500−800 MHz wide (see Figure 16). Compared to Figure 15, it is evident that multiband UWB can make more efficient use of the FCC mask, minimize interference to existing narrowband systems by flexible band selection, and facilitate future scalability of the spectrum use. Moreover, since each band occupies only a fraction of the bandwidth of a single-band transmission, the pulse shaper employed in multiband UWB can have much longer duration in time, which in turn eases implementation of the ADC, and enables implementation with off-the-shelf (OTS) components capitalizing on existing mature technology for wideband communications.

As in single-band UWB, challenges facing multiband UWB systems include timing acquisition and channel estimation. The (non)data aided timing algorithms for synchronization, and channel estimators, including TDT, TR and PWAM, we outlined for single-band UWB apply also to multiband alternatives on a per band basis. However, due to the introduction of multiple carrier frequencies, new challenges arise. Recall that in the baseband MC-UWB systems, multiple *digital* subcarriers are utilized; whereas multiband UWB radios rely on *analog* carriers, and thus have to deal with multiple carrier frequency offsets (CFO) arising from the mismatch of multiple transmit-receive oscillators. Unless compensated for, CFO is known to degrade performance severely, especially in carrier-modulated MC-UWB transmissions. For multiband UWB, carrier frequency synchronization is more challenging because there are more than one carrier frequencies, especially when OFDM or fast frequency-hopping is employed across multiple bands. For this reason, multiband UWB calls for CFO sensitivity studies, low complexity CFO estimators, and per-subcarrier based channel estimation modules. To this end, existing techniques for wideband communications can serve as starting points.

Multiband UWB multiple access schemes also have to be designed by taking all bands into consideration. Notice that the carrier frequencies (center frequencies) of subbands in Figure 16 span a wide range from 3.35 GHz up to 10.35 GHz with a 500 MHz multiband partitioning. Consequently, the bands to the right (towards the 10.6 GHz end) tend to be more lossy than the bands to the left (towards the 3.1 GHz end). Therefore, an assignment confining each user to a single fixed band will result in user-dependent performance, and will not enable the full multipath diversity. In a nutshell, a multiband based UWB-MA scheme must account for the following issues: i) flexibility to accommodate various schemes (SC or MC) for multiple access, ii) capability to collect full multipath diversity, and iii) scalability in spectral efficiency (from low, to medium, and high data rates).

Cross-Band FLEX-UWB Access

To meet the aforementioned requirements, we have recently introduced a cross-band flexible UWB MA scheme for high-rate multipiconet WPANs [80]. The so termed FLEX-UWB design is built on the basis of the MSBS-UWB approach we outlined earlier to achieve resilience against MUI in an environment with multiple piconets. To allow for various selections of spreading codes, FLEX-UWB relies on an FFT matrix $\boldsymbol{F}_{N_s}$, of size $N_s \times N_s$, where N_s denotes the number of

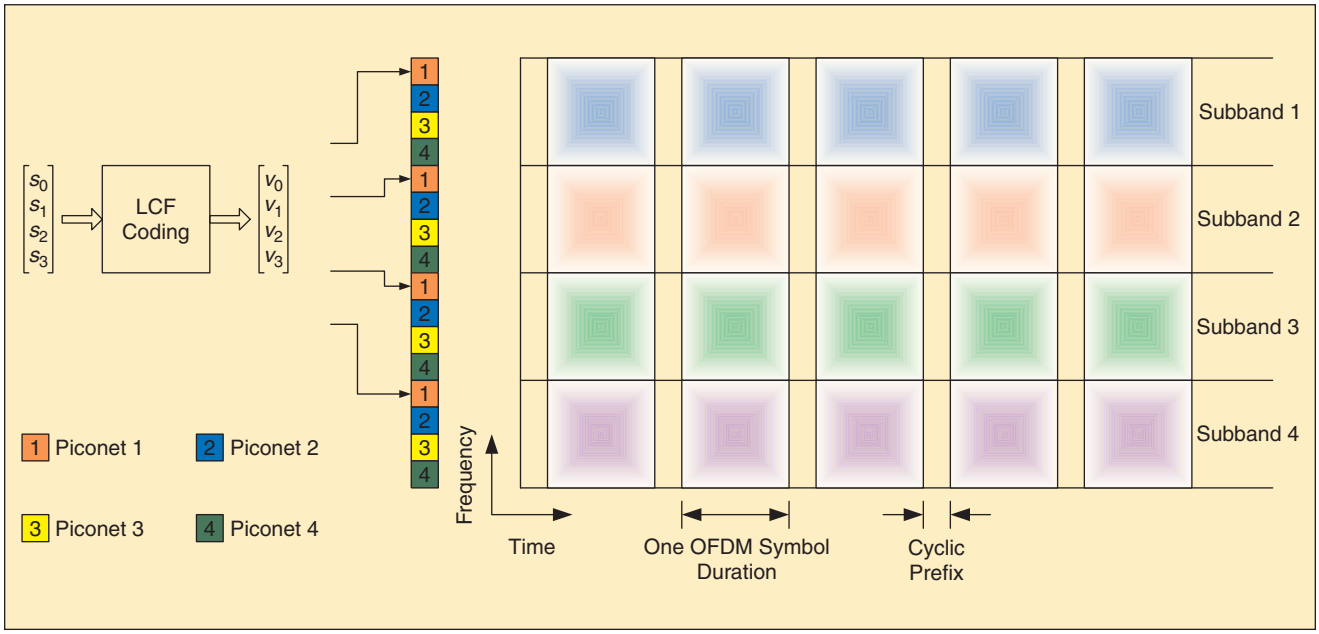

▲ *17. FLEX-UWB: cross-band LCF-OFDMA (s_k: symbols; v_k: coded symbols; number of subbands: 4; number of piconets: 4; total number of users $N_u = 4$; number of subcarriers per subband $N_s = 4$).*

subcarriers per subband. Let N_u denote the total number of users across all piconets, and define $P := N_s/N_u$. Built on the user-specific $N_u \times 1$ spreading code $\boldsymbol{c}_u$, the basic block-spreading matrix is given by

$$\boldsymbol{C}_u := \left[\boldsymbol{F}_{N_s}^{\mathcal{H}}(\boldsymbol{c}_u \otimes \boldsymbol{I}_P)\right] \otimes \boldsymbol{T}_{zp}, \qquad (25)$$

where $\boldsymbol{I}_P$ is a $P \times P$ identity matrix, and $\boldsymbol{T}_{zp}$ is a $(K + L_d) \times K$ matrix that pads L_d zeros to a $K \times 1$ vector, with K being the size of information symbol blocks, and L_d denoting the order of the discrete-time equivalent channel. The resulting multiple access scheme depends on the selection of the spreading codes $\{\boldsymbol{c}_u\}_{u=0}^{N_u-1}$. Time-division multiple access (TDMA), where each user utilizes the whole bandwidth at different time slots, can be achieved by choosing $\{\boldsymbol{c}_u\}_{u=0}^{N_u-1}$ as columns of FFT matrix $\boldsymbol{F}_{N_u}$, of size $N_u \times N_u$. Choosing the spreading codes as columns of a $N_u \times N_u$ identity matrix results in frequency-division multiple access (FDMA), where each user utilizes part of the bandwidth but can transmit all the time. And with $\{\boldsymbol{c}_u\}_{u=0}^{N_u-1}$ being any set of mutually orthogonal vectors, code-division multiple access (CDMA) can be achieved, where each user utilizes the entire bandwidth all the time with a user-specific signature. It turns out that the code design (25) can be applied simultaneously over all (or, selected) subbands, and guarantees: i) MUI-resilient UWB-MA; ii) full multipath diversity; and iii) bandwidth efficiency of $K/(K + L_d)$ [117]. Notice that the bandwidth efficiency of FLEX-UWB is the same as that of MSBS-UWB, and is tunable by varying the symbol block size K, which also affects the decoding delay.

As mentioned before, choosing $\{\boldsymbol{c}_u\}$ to be columns of the identity matrix $\boldsymbol{I}_{N_u}$ gives rise to FDMA. In particular, replacing $\boldsymbol{T}_{zp}$ with an identity matrix $\boldsymbol{I}_K$, and selecting $K = 1$, (25) boils down to: $\boldsymbol{C}_u = \boldsymbol{F}_{N_s}^{\mathcal{H}}(\boldsymbol{c}_u \otimes \boldsymbol{I}_P)$. Such a code design, coupled with cyclic-prefix insertion (removal) at the transmitter (receiver), corresponds to an orthogonal (O)FDMA UWB scheme, where each user occupies all P subcarriers of each subband [80]. It is well known that OFDMA can be implemented efficiently with the FFT module, but has to resort to (possibly considerable) bandwidth overexpansion to mitigate frequency-selective fading. To amend this problem, a cross-band linear complex field (LCF) precoder is also introduced in [80]. (For tutorial treatments of LCF (pre)coding, the reader is referred to [30] and [67].) The transmission corresponding to FLEX-UWB with the LCF-OFDMA choice is depicted in the example of Figure 17, where each subband consists of $N_s = 4$ subcarriers, the first of which is assigned to piconet 1. The number of information symbols per block is four, which is the total number of subcarriers (across all subbands) assigned to a single piconet. The symbol block is first passed through an LCF encoder (a square matrix), whose output is the coded symbol block $\boldsymbol{v}$. Notice that no redundancy is introduced here. The coded symbol block $\boldsymbol{v}$ is then evenly distributed to all subbands and transmitted using an OFDMA scheme, which consists of selecting user-specific subcarriers, inverse FFT, and cyclic-prefix insertion.

Capacity in the UWB Regime

Shortly after his landmark paper [53], Shannon pointed out that as the bandwidth B grows, the AWGN channel capacity approaches:

$$C_{\text{AWGN}}^{\infty} := \lim_{B\to\infty} C_{\text{AWGN}}(B) = \lim_{B\to\infty} B\log\left(1+\frac{\mathcal{P}}{BN_0}\right) = \frac{\mathcal{P}}{N_0}\log e,$$

where $\mathcal{P}$ is the received power and $N_0/2$ is the noise PSD. Evidently, given N_0 and $\mathcal{P}$, C_{AWGN}^{∞} benchmarks the maximum rate achievable. But how close practical UWB systems come to this fundamental limit? And how UWB transceivers should be designed to approach it? For *flat* Rayleigh fading channels, it is known that as $B\to\infty$, C_{AWGN}^{∞} can be achieved by frequency shift keying [17].

But as we discussed in Section III-A, UWB transmissions typically encounter *multipath* fading channels. This motivates investigation of capacity issues for UWB channels with pronounced frequency selectivity. If such channels exhibit independent fading at different frequency bins, it turns out that the achievable mutual information for a fixed transmission power goes to zero as B increases, when spread spectrum signaling is used [33]. This result is quite intuitive because independent fading across frequency bins together with an increasing B implies infinite number of independent multipath coefficients, whose estimation then exhausts the power and bandwidth resources. But Figures 2 and 3 suggest that even when the number of *resolvable* multipath returns ($\tilde{L}$) increases with increasing B (decreasing T_p), the total number of paths ($L+1$) induced by the physical surroundings is practically finite. Let $\{d_l,\beta_l\}_{l=1}^{\tilde{L}}$ denote the delays and coefficients of the *resolvable* paths. Notice that $\{d_l,\beta_l\}_{l=1}^{\tilde{L}}$ depend on, but are not necessarily identical to, the delays and coefficients of the physical channel $\{\tau_l,\alpha_l\}_{l=0}^{L}$. Evidently, $\tilde{L}$ is upper bounded by $(L+1)$ as B increases. To investigate the capacity behavior in such cases, consider a white-noise-modulation (WNM) signaling where the empirical autocorrelation of the transmitted waveform resembles that of white noise, and a quasi-static channel with coherence time τ_c and maximum delay spread $\tau_{L,0}\ll\tau_c$. Then the following results are obtained in [58]:

▲ a) When $\{d_l\}_{l=1}^{\tilde{L}}$ are known but $\{\beta_l\}_{l=1}^{\tilde{L}}$ are unknown, the achievable mutual information using WNM signaling is lower and upper bounded by $[1-(\tilde{L}/\tilde{L}_c)\times\log(1+\tilde{L}_c/\tilde{L})]C_{\text{AWGN}}^{\infty}$ and $(\tilde{L}_c/\tilde{L})C_{\text{AWGN}}^{\infty}$, respectively, where $\tilde{L}_c := \mathcal{P}\tau_c/N_0$. Consequently, if $\tilde{L}\ll\tilde{L}_c$ then $(\tilde{L}/\tilde{L}_c)\log(1+\tilde{L}_c/\tilde{L})\approx 0$ and the achievable mutual information approaches C_{AWGN}^{∞}; whereas if $\tilde{L}\gg\tilde{L}_c$ then $\tilde{L}_c/\tilde{L}\approx 0$ and the achievable mutual information is negligibly small.

▲ b) When $\{d_l\}_{l=1}^{\tilde{L}}$ are unknown (regardless of whether $\{\beta_l\}_{l=1}^{\tilde{L}}$ are known or not), the upper bound on the mutual information using WNM signaling decays to 0 like $1/B$, even when $\tilde{L}=1$ and β_1 is known.

In result a), $\tilde{L}_c$ essentially captures the available resources, namely the SNR $\mathcal{P}/N_0$ and the coherence time τ_c. As $\tilde{L}$ increases, more unknowns $\{d_l,\beta_l\}_{l=1}^{\tilde{L}}$ need to be estimated. If the number of unknowns is too large, negligible resources remain for conveying information, which drives the mutual information to zero. An intuitive explanation is also possible for result b). As $\{d_l\}_{l=1}^{\tilde{L}}$ represent delays of resolvable paths, one delay can be distinguished from its neighbors by the pulse duration T_p. But this requires timing estimation (tracking) with pulse-resolution accuracy. Since $T_p\approx 1/B$, it is expected that the resources will again be depleted by such stringent tracking requirements. As an extreme example, consider $\tilde{L}=1$ with β_1 known. In this case, finding d_1 amounts to the timing synchronization problem. As discussed earlier, reliable symbol recovery is impossible once the waveform of duration T_p is missed. As B grows, it is becoming increasingly difficult to capture the shrinking pulse.

To fulfill expectations, UWB research and development has to cope with formidable challenges that limit their bit error rate performance, capacity, throughput, and network flexibility.

The capacity results a) and b) corroborate the demanding and challenging nature of UWB timing synchronization and channel estimation. They indicate that receiver knowledge of $\{d_l\}_{l=1}^{\tilde{L}}$ is particularly critical in achieving capacity. The question is when the assumptions under a) are satisfied; i.e., when can $\{d_l\}_{l=1}^{\tilde{L}}$ be treated as known at the receiver? We know that $\tau_c\propto 1/f_c$ and that the time it takes for β_l to move by one tap (from d_l to d_l+T_p) is proportional to $T_p\approx 1/B$. Therefore, when $1/B\gg 1/f_c$, the resolvable delays $\{d_l\}_{l=1}^{\tilde{L}}$ change much slower than the corresponding coefficients $\{\beta_l\}_{l=1}^{\tilde{L}}$ and can be treated as if they can be "tracked" at the receiver. In other words, result a) requires the fractional bandwidth satisfy $B/f_c\ll 1$. This may be the case with multiband UWB systems with relatively large f_c, but is not satisfied by baseband UWB systems.

The spread-spectrum and WNM systems we discussed so far use transmissions with no duty cycle; i.e., $T_f=T_p$. In low-duty-cycle UWB systems, however, we have $T_f\gg T_p$. How does duty-cycling affect capacity in the UWB regime? Let us first define the duty-cycle parameter θ: with $\theta\in(0,1]$, transmission occurs only during one period τ_c out of the total of τ_c/θ seconds; and the system sleeps when not transmitting. Interestingly, as FSK that is "peaky" in frequency is

capacity achieving in flat-fading channels, duty-cycled signals that are "peaky" in time are capacity achieving in multipath channels [41], [65]. In fact, it follows from results a) and b) that WNM and PPM can both achieve C^{∞}_{AWGN} when they are "duty-cycled" with $\theta \to 0$ [41]:

▲ A) As long as $\{d_l\}_{l=1}^{\tilde{L}}$ are *known* at the receiver, then

$$\lim_{B\to\infty} C_{\text{WNM}}(B) \to C^{\infty}_{\text{AWGN}}, \quad \text{if } \lim_{B\to\infty} \tilde{L}/B \to 0,$$

$$\lim_{B\to\infty} C_{\text{PPM}}(B) \to C^{\infty}_{\text{AWGN}}, \quad \text{if } \lim_{B\to\infty} \tilde{L}\log\log B/\sqrt{\log B} \to 0.$$

▲ B) If $\{d_l\}_{l=1}^{\tilde{L}}$ are also *unknown* at the receiver, then

$$\lim_{B\to\infty} C_{\text{WNM}}(B) \begin{cases} \to C^{\infty}_{\text{AWGN}}, \\ \text{if } \lim_{B\to\infty} \tilde{L}\log B/B \to 0 \\ < C^{\infty}_{\text{AWGN}}, \\ \text{if } \lim_{B\to\infty} \tilde{L}/B \to \lambda > 0, \end{cases}$$

$$\lim_{B\to\infty} C_{\text{PPM}}(B) \begin{cases} \to C^{\infty}_{\text{AWGN}}, \\ \text{if } \tilde{L} = 1 \\ \to 0, \\ \text{if } \lim_{B\to\infty} \tilde{L}/\log B \to \infty. \end{cases}$$

Notice that WNM and PPM signaling systems can tolerate different bandwidth scaling factors as the number of resolvable paths $\tilde{L}$ increases. Also, when timing knowledge is not available, these factors are further reduced. These results are established for real UWB channels with $\{\beta_l\}_{l=1}^{\tilde{L}}$ being i.i.d. It would be interesting to see how the correlation and power profile of the channel affect these scaling factors.

UWB at the Networking Layer

Along with flexibility requirements at the physical layer, the open access network paradigm requires redefinition of upper layers in the UWB system architecture. In the same way Internet protocol (IP) has succeeded in gluing together heterogeneous networks, UWB and the open radio access paradigm offer the potential for integrating heterogeneous wireless access networks. To reach this goal, one needs to first address the following question regarding the next-to-physical medium access control (MAC) layer: What, if any, UWB specific features may be required within the MAC?

Utilizing TH, conventional UWB systems provide covertness and are considered as the physical layer for future tactical wireless networks [24]. However, the high precision synchronization required by UWB systems necessitates long acquisition headers at higher power, especially when simple serial searching algorithms are adopted due to the size and processing power of UWB transceivers. To improve covertness in a UWB-based network, sustained link networks (SLN) were proposed in [24] as a MAC layer scheme. In SLN, the physical layer links are maintained for the lifetime of the logical link between two nodes. Taking advantage of the low duty-cycle nature of conventional UWB communications, especially at low bit rate, [24] also developed a full-duplex scheme, which results in a tradeoff between the number of transceiver units and the bit rate.

UWB allows for accurate localization, especially in environments where GPS encounters satellite visibility constrains. Such a precise positioning information can be utilized to develop location-aware networking. In other words, improved coexistence with other piconets/systems and reduced power consumption can be achieved by scaling personal operating space based on UWB localization. Furthermore, for a prescribed average power, the peak power is inversely proportional to the pulse repetition frequency (PRF), which induces a range-rate tradeoff. Based on accurate localization information, a promising direction for UWB systems is to adjust data rates on a per packet, or a per link basis. As a result, the unique features of UWB may lead to power-efficient, location-aware adaptive routing protocols.

Fast timing techniques will allow for quick computation and tracking of the relative positions among sensors, which would be beneficial for position-assisted node selection, and information relaying with minimum energy consumption. Idle or partially functional nodes can also be utilized as relays to ensure fault-tolerant networking. This approach has the potential to improve performance, while saving power.

To facilitate variable bit rate sessions and fair-queuing bandwidth guarantees (those cannot be simultaneously accommodated by fixed-assignment or random access alternatives), a two-phase demand assignment MAC could be pursued. This layer-integrating design could start at the network scheduling which is to be performed by the "master user" of the piconet. Similar to a generalized process sharing policy [38], [49], [56], the scheduler associates "slave user" u with a service-dependent weight F_u that determines percentage of bandwidth allocation B_u. During the first phase (TDMA contention based reservation), the intention of the slave user to transmit along with the requested F_u is communicated to the scheduler via mini-slots, while the master user responds with mini-slots containing each user's ID with the corresponding code assignment. During the second phase, users transmit (possibly at different rates) multimedia information. The MSBS and FLEX spreading codes we outlined earlier are good choices for this stage, because they not only assure MUI/multipath-resilient operation but also enable multirate transmissions with full-diversity, fine rate resolution, and easy rate switching capability [67], [76], [80].

Existing dynamic resource allocation schemes could also be adopted to UWB settings, especially when location information and partial channel state information (CSI) become available (or can be predicted) at the trans-

mitter. Optimization criteria can involve maximization of sum-capacity, or, minimization of symbol error rate bounds, under a prescribed transmit-power budget. Moreover, ST codes and/or steerable antenna arrays (beamformers) can also be adjusted for packet-fair scheduling and flexible UWB allocation along the lines of [78].

Another interesting direction is to couple resource allocation with routing considerations by distributing resources among nodes in an optimal fashion. On these subjects, one of the key elements is the exploitation of information from lower layers. For example, link quality maps provided by the channel estimation and error control algorithms are expected to play a critical role in routing establishment. Due to channel fading, routes in a wireless network are inherently unstable and prone to link failures. This has an adverse effect on the ability of networks to support applications with stringent quality of service (QoS) requirements. Exploitation of the extra diversity offered by multipath routes of the UWB channel calls for an analytical framework for multipath routing in (un)coordinated networking environment. For UWB links, multipath routing is particularly attractive, because it can provide path failure protection, load balancing, while at the same time reduce the transmission delay by distributing traffic among a set of available paths.

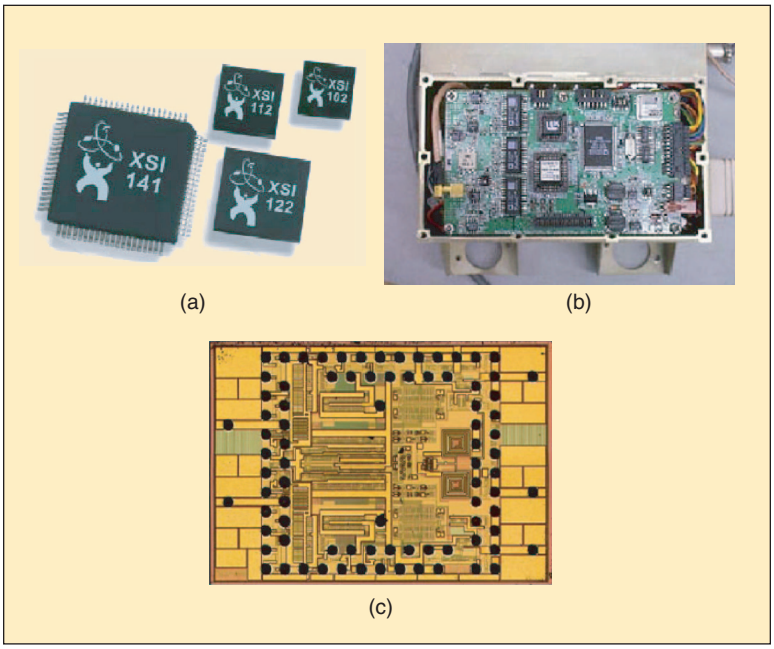

▲ *18. (a) The Trinity chip set released by Xtreme Spectrum Inc.; (b) The Mobile ad hoc Network (MANET) by MultiSpectral Solutions Inc.; (c) the PUlsON family marketed by Time Domain Corporation.*

Implementation Issues

Any practical UWB system design should take into account implementation feasibility and complexity issues, including ADC speed and correlator bandwidth. An overview on these issues can be found in [18]. In particular, to reduce time-to-market, UWB designs with analog components should utilize commonplace building blocks, e.g., low noise amplifiers (LNAs), mixers, ADCs, digital-to-analog converters (DACs), and phase locked loops (PLLs), for which standard figure of merit production tests are available. Currently, analog/RF circuits are mostly implemented in high performance SiGe platforms, whereas digital/base-band circuits are implemented in CMOS. The latter is superior in terms of both power consumption and cost. At the same time, DSP based designs also enjoy process portability, low sensitivity to component variability, as well as benefits from Moore's law. A system design free of RF components will facilitate system-on-a-chip (SoC) implementation in CMOS, which shrinks as CMOS scales down from 0.18 μm to 0.13 μm and 0.09 μm. In this aspect, different system designs score differently. The conventional single-band UWB systems mostly rely on base-band carrier-free transmissions, and therefore require no IF processing. Whereas the recently emerged multiband UWB systems utilize the FCC mask more effectively, but entail more extensive IF processing at rather high frequencies, and a number of oscillators at both the transmitter and the receiver. For any given UWB system, comparative studies need to be carried out when multiple implementation alternatives (analog versus digital) exist. For instance, channel estimation and correlation in TDT, TR, and PWAM systems can be implemented either with analog delay lines, or, with digital delay elements after AD converting the analog waveform. Avoiding analog delay lines, the latter requires formidable sampling. Analyses and tradeoff studies of these alternatives are either performed [8], [81], or are underway [23]. It is also worth mentioning that the complexity reduction at higher hierarchies is often times more effective than at lower hierarchies. For instance, about 60% of the total number of gates are dedicated to channel estimation. This number can certainly be reduced to some degree by applying digital circuit design techniques. On the other hand, adopting more efficient channel estimation techniques might reduce dramatically the number of gates. These are areas where VLSI-SP expertise can have considerable impact in UWB algorithms and implementation.

System designs tailored for UWB as mentioned in preceding sections also entail challenges to UWB circuitry implementation. Successful implementation of both carrier-free baseband and carrier-modulated multiband UWB calls for high-efficiency UWB antennas, and tight jitter requirements. To this end, there is a rich literature in UWB Radar, and emerging works in communications. High-rate transmissions require fast automatic gain control (AGC) response, as well as improved ADC

speed. In [35], a channelized ADC with CMOS implementation is advocated. As mentioned before, multiband solutions with carrier modulated pulses utilize the FCC allowable bandwidth efficiently. Hopping among multiple frequency bands requires high performance local oscillators and switching circuits as well as UWB antennas. Implementation of such systems with low power consumption and low cost requires integration of RF and baseband circuitry into a single CMOS chip, which hinges upon the solution of the "touchy issue" of substrate noise mitigation. Further development of UWB systems will also benefit from increased SP expertise to enable modulation/demodulation, synchronization, channel estimation, error control coding, as well as cross-layer functionalities.

A number of companies have already announced UWB prototype products for various applications: the Trinity chip set released by Xtreme Spectrum Inc. for streaming video applications; the Mobile ad hoc Network (MANET) by MultiSpectral Solutions Inc.; and the PulsON family marketed by Time Domain Corporation for personnel and asset tracking systems (see Figure 18).

Closing Remarks

Just a year after announcing the First R&O, FCC affirmed rules to authorize the deployment of UWB technology and sponsored several demonstrations of UWB devices on 13 February 2003. During this assemblage, seven companies demonstrated 12 UWB systems, which cover applications from communications, through-wall and/or ground-penetrating Radar, and localization. At the same time, a number of special issues in journals and special sessions in various conferences are devoted to UWB research and development. IEEE sponsors a Working Group for standardization and a biennial workshop in Ultra-Wideband Systems and Technology (UWBST), where the number of signal processing and communications researchers increases rapidly. All these justify well that indeed UWB is an idea "whose time has come."

To realize this idea, however, UWB research and development has to cope with challenges that limit their performance, capacity, throughput, network flexibility, implementation complexity, and cost. Those include precise and rapid synchronization in a multiuser (and possibly ad hoc) environment, modeling of UWB channel variations, low complexity channel estimation and multipath diversity collection, UWB-MA schemes that facilitate MUI/NBI suppression, and their corresponding multi-user detectors, UWB-tailored MAC layer schemes, high-speed high-precision A/D and D/A converter designs, high-frequency oscillators, and high efficiency UWB antennas.

To fully exploit the benefits of UWB systems, enhanced interdisciplinary links need to be established across the signal processing, communications, and networking communities. Today, research in signal processing for UWB is still at its infancy, offering limited resources in handling the challenges facing UWB communications. On the other hand, digital signal processing techniques have matured for conventional RF communications, and a large body of literature has grown from recent advances in narrowband and wideband wireless communications. Understanding the unique properties and challenges of UWB communications, and applying competent signal processing techniques are vital to conquering the obstacles towards developing exciting UWB applications. It is clear that innovative research in this area will pay handsome dividends in meeting the future challenges and demands of the dynamic communications industry.

Acknowledgments

This article was prepared through collaborative participation in the Communications and Networks Consortium sponsored by the U.S. Army Research Laboratory under the Collaborative Technology Alliance Program, Cooperative Agreement DAAD19-01-02-0011. This work was also supported by the NSF Grant EIA-0324864.

Liuqing Yang received her B.S. degree in electrical engineering from Huazhong University of Science and Technology, Wuhan, China, in 1994, and her M.Sc. and Ph.D. degrees in electrical and computer engineering from the University of Minnesota in 2002 and 2004, respectively. Since August 2004, she has been an assistant professor with the Department of Electrical and Computer Engineering at the University of Florida. Her general research interests include communications, signal processing and networking. Currently, she has a particular interest in ultra-wideband communications. Her research encompasses synchronization, channel estimation, equalization, multiple access, space-time coding, and multicarrier systems.

Georgios B. Giannakis received his diploma in electrical engineering from the National Technical University of Athens, Greece, in 1981 and an M.Sc. in electrical engineering in 1983, an M.Sc. in mathematics in 1986, and a Ph.D. in electrical engineering in 1986, all from the University of Southern California. He joined the University of Virginia in 1987. Since 1999 he has been a professor with the Department of Electrical and Computer Engineering at the University of Minnesota, where he holds an ADC Chair in Wireless Telecommunications. His general interests span the areas of communications and signal processing, estimation and detection theory, time-series analysis, and system identification, on which he has published more than 200 journal papers, 350 conference papers, and two edited books. He received many awards, including the 2000 IEEE Signal Processing Society's Technical Achievement Award. He was editor-in-chief for *IEEE Signal Processing Letters*, associate editor for *IEEE Transactions on Signal Processing*, and served many

positions within the IEEE Signal Processing Society, including secretary of the Conference Board and member of the Publications Board and the Board of Governors. He is also a member of the *Proceedings of the IEEE* editorial board and the steering committee of *IEEE Transactions on Wireless Communications.*

References

[1] G.R. Aiello and G.D. Rogerson, "Ultra-wideband wireless systems," *IEEE Microwave Mag.*, vol. 4, no. 2, pp. 36–47, 2003.

[2] I.F. Akyildiz, W. Su, Y. Sankarasubramaniam, and E. Cayirci, "A survey on sensor networks," *IEEE Commun. Mag.*, vol. 40, no. 8, pp. 102–114, 2002.

[3] S.M. Alamouti, "A simple transmit diversity technique for wireless communications," *IEEE J. Select. Areas Commun.*, vol. 16, no. 8, pp. 1451–1458, 1998.

[4] J. Balakrishnan, A. Batra, and A. Dabak, "A multi-band OFDM system for UWB communication," in *Proc. Conf. Ultra-Wideband Systems and Technologies*, Reston, VA, 2003, pp. 354–358.

[5] T.W. Barrett, "History of ultra wideband (UWB) radar and communications: Pioneers and innovators," in *Proc. Progress in Electromagnetics Symposium*, Cambridge, MA, 2000.

[6] C. Carbonelli, U. Mengali, and U. Mitra, "Synchronization and channel estimation for UWB signals," in *Proc. Global Telecommunications Conf.*, San Francisco, CA, 2003, pp. 764–768.

[7] Y. Chao and R.A. Scholtz, "Optimal and suboptimal receivers for Ultra-wideband transmitted reference systems," in *Proc. Global Telecommunications Conf.*, San Francisco, CA, 2003, pp. 744–748.

[8] J.D. Choi and W.E. Stark, "Performance of ultra-wideband communications with suboptimal receivers in multipath channels," *IEEE J. Select. Areas Commun.*, vol. 20, no. 9, pp. 1754–1766, 2002.

[9] C.R.C.M. da Silva and L.B. Milstein, "Spectral-encoded UWB communication systems," in *Proc. Conf. Ultra-Wideband Systems and Technologies*, Reston, VA, 2003, pp. 96–100.

[10] G. Durisi and G. Romano, "On the validity of Gaussian approximation to characterize the multiuser capacity of UWB TH PPM," in *Proc. Conf. Ultra-Wideband Systems and Technologies*, Baltimore, MD, 2002, pp. 157–161.

[11] G. Durisi, A. Tarable, J. Romme, and S. Benedetto, "A general method for error probability computation of UWB systems for indoor multiuser communications," *J. Commun. Networks*, vol. 5, no. 4, pp. 354–364, 2003.

[12] FCC First Report and Order: In the matter of Revision of Part 15 of the Commission's Rules Regarding Ultra-Wideband Transmission Systems, *FCC 02–48*, April 2002.

[13] R. Fleming, C. Kushner, G. Roberts, and U. Nandiwada, "Rapid acquisition for Ultra- Wideband localizers," in *Proc. Conf. Ultra-Wideband Systems and Technologies*, Baltimore, MD, 2002, pp. 245–250.

[14] J.R. Foerster, Channel Modeling Sub-committee Report Final, IEEE P802.15-02/368r5-SG3a, IEEE P802.15 Working Group for WPAN, 2002.

[15] J.R. Foerster, "The performance of a direct-sequence spread ultra wideband system in the presence of multipath, narrowband interference, and multiuser interference," in *Proc. Conf. Ultra-Wideband Systems and Technologies*, Baltimore, MD, 2002, pp. 87–92.

[16] A.R. Forouzan, M. Nasiri-Kenari, and J.A. Salehi, "Performance analysis of time-hopping spread-spectrum multiple-access systems: Uncoded and coded schemes," *IEEE Trans. Wireless Commun.*, vol. 1, no. 4, pp. 671–681, 2002.

[17] R.G. Gallager, *Information Theory and Reliable Communication.* New York: Wiley, 1968.

[18] R. Harjani, J. Harvey, and R. Sainati, "Analog/RF physical layer issues for UWB systems," in *Proc. the 17th Int. Conf. VLSI Design*, Mumbai, India, 2004, pp. 941–948.

[19] M. Ho, V. Somayazulu, J. Foerster, and S. Roy, "A differential detector for an Ultra-Wideband communications system," in *Proc. Vehicular Technology Conf.*, Birmingham, AL, 2002, pp. 1896–1900.

[20] B.M. Hochwald and T.L. Marzetta, "Unitary space-time modulation for multiple-antenna communications in Rayleigh flat fading," *IEEE Trans. Inform. Theory*, vol. 46, no. 2, pp. 543–564, 2000.

[21] R.T. Hoctor and H.W. Tomlinson, "An overview of delay-hopped, transmitted-reference RF communications," in *G.E. Research and Development Center, Technical Information Series*, 2002, pp. 1–29.

[22] E.A. Homier and R.A. Scholtz, "Rapid acquisition of Ultra-Wideband signals in the dense multipath channel," in *Proc. Conf. Ultra-Wideband Systems and Technologies*, Baltimore, MD, 2002, pp. 105–110.

[23] S. Hoyos, B. Sadler, and G. Arce, "On the performance of low complexity digital receivers for Ultra-Wideband communication systems," in *Proc. Collaborative Tech. Alliances Conf.*, College Park, MD, 2003, pp. 211–215.

[24] S.S. Kolenchery, K. Townsend, and J.A. Freebersyser, "A novel impulse radio network for tactical wireless communications," in *Proc. MILCOM Conf.*, Bedford, MA, 1998, pp. 59–65.

[25] H. Lee, B. Han, Y. Shin, and S. Im, "Multipath characteristics of impulse radio channels," in *Proc. Vehicular Technology Conf.*, Tokyo, Japan, Spring 2000, pp. 2487–2491.

[26] J.S. Lee, C. Nguyen, and T. Scullion, "New uniplanar subnanosecond monocycle pulse generator and transformer for time-domain microwave applications," *IEEE Trans. Microwave Theory Tech.*, vol. 49, no. 6, pp. 1126–1129, 2001.

[27] Q. Li and L.A. Rusch, "Multiuser detection for DS-CDMA UWB in the home environment," *IEEE J. Select. Areas Commun.*, vol. 20, no. 9, pp. 1701–1711, 2002.

[28] V. Lottici, A. D'Andrea, and U. Mengali, "Channel estimation for ultra-wideband communications," *IEEE J. Select. Areas Commun.*, vol. 20, no. 9, pp. 1638–1645, 2002.

[29] X. Luo, L. Yang, and G.B. Giannakis, "Designing optimal pulse-shapers for ultra-wideband radios," *J. Commun. Networks*, vol. 5, no. 4, pp. 344–353, 2003.

[30] X. Ma and G.B. Giannakis, "Complex field coded MIMO systems: Performance, rate, and tradeoffs," *Wireless Commun. Mobile Comput.*, vol. 2, no. 7, pp. 693–717, 2002.

[31] I. Maravić, J. Kusuma, and M. Vetterli, "Low-sampling rate UWB channel characterization and synchronization," *J. Commun. Networks*, vol. 5, no. 4, pp. 319–327, 2003.

[32] C.L. Martret and G.B. Giannakis, "All-digital impulse radio for wireless cellular systems," *IEEE Trans. Commun.*, vol. 50, no. 9, pp. 1440–1450, 2002.

[33] M. Médard and R.G. Gallager, "Bandwidth scaling for fading channels," *IEEE Trans. Inform. Theory*, vol. 48, no. 4, pp. 840–852, 2002.

[34] U. Mengali and A. D'Andrea, *Synchronization Techniques for Digital Receivers.* New York: Plenum, 1997.

[35] W. Namgoong, "A channelized digital ultrawideband receiver," *IEEE Trans. Wireless Commun.*, vol. 2, no. 3, pp. 502–510, 2003.

[36] S. Ohno and G.B. Giannakis, "Capacity maximizing MMSE-optimal pilots and precorders for wireless OFDM over rapidly fading channels," *IEEE Trans. Inform. Theory*, vol. 50, no. 9, pp. 2138–2145, 2004.

[37] Assessment of Ultra-Wideband (UWB) Technology, OSD/DARPA, Ultra-Wideband Radar Review Panel, R-6280, July 13, 1990.

[38] A.K. Parekh and R.G. Gallager, "A generalized processor sharing approach to flow control in integrated services networks: The single-node case," *IEEE/ACM Trans. Networking*, vol. 1, no. 3, pp. 344–357, 1993.

[39] T.W. Parks and J.H. McClellan, "Chebyshev approximation for nonrecursive digital filters with linear phase," *IEEE Trans. Circuit Theory*, vol. 19, no. 2, pp. 189–194, 1972.

[40] B. Parr, B. Cho, K. Wallace, and Z. Ding, "A novel ultra-wideband pulse design algorithm," *IEEE Commun. Letters.*, vol. 7, no. 5, pp. 219–221, 2003.

[41] D. Porrat and D. Tse, "Bandwidth scaling in ultra wideband communications," in *Proc. 41st Allerton Conf.*, Univ. of Illinois at U-C, Monticello, IL, 2003.

[42] J. Proakis, *Digital Communications*, 4th ed. New York: McGraw-Hill, 2001.

[43] F. Ramirez-Mireles and R.A. Scholtz, "N-orthogonal time-shift-modulated signals for ultra wide bandwidth impulse radio modulation," in *Proc. IEEE Mini Conf. Communication Theory*, Phoenix, AZ, 1997, pp. 245–250.

[44] J. Romme and L. Piazzo, "On the power spectral density of time-hopping impulse radio," in *Proc. Conf. Ultra-Wideband Systems and Technologies*, Baltimore, MD, 2002, pp. 241–244.

[45] G.F. Ross, "The transient analysis of multiple beam feed networks for array systems," Ph.D. dissertation, Polytechnic Institute of Brooklyn, Brooklyn, NY, 1963.

[46] G.F. Ross and K.W. Robbins, Base-band radiation and reception system, U.S. Patent 3,739,392, June 12, 1973.

[47] E. Saberinia and A.H. Tewfik, "Pulsed and non-pulsed OFDM Ultra Wideband wireless personal area networks," in *Proc. Conf. Ultra-Wideband Systems and Technologies*, Reston, VA, 2003, pp. 275–279.

[48] B.M. Sadler and A. Swami, "On the performance of UWB and DS -spread spectrum communication systems," in *Proc. Conf. Ultra-Wideband Systems and Technologies*, Baltimore, MD, 2002, pp. 289–292.

[49] D. Saha, S. Mukherjee, and S.K. Tripathi, "Carry-over round robin: a simple cell scheduling mechanism for ATM networks," *IEEE Trans. Networking*, vol. 6, no. 6, pp. 779–796, 1998.

[50] A.A.M. Saleh and R.A. Valenzuela, "A statistical model for indoor multipath propagation," *IEEE J. Select. Areas Commun.*, vol. 5, no. 2, pp. 128–137, 1987.

[51] H.G. Schantz and L. Fullerton, "The diamond dipole: A Gaussian impulse antenna," in *Proc. IEEE Int. Symp. Antennas and Propagation Society*, vol. 4, Boston, MA, 2001, pp. 100–103.

[52] R.A. Scholtz, "Multiple access with time-hopping impulse modulation," in *Proc. MILCOM Conf.*, Boston, MA, 1993, pp. 447–450.

[53] C.E. Shannon, "A mathematical theory of communication," *Bell Syst. Tech. J.*, vol. 27, pp. 379–423, 623–656, 1948.

[54] M.K. Simon, *Spread Spectrum Communications Handbook*. New York: McGraw-Hill, 1985.

[55] E.M. Staderini, "UWB radars in medicine," *IEEE Aerosp. Electron. Syst. Mag.*, vol. 17, no. 1, pp. 13–18, 2002.

[56] A. Stamoulis and G.B. Giannakis, "Deterministic time-varying packet fair queueing for integrated services networks," *J. VLSI Signal Processing*, vol. 30, no. 1–3, pp. 71–87, 2002.

[57] J.D. Taylor, *Ultra Wideband Radar Technology*. New York: CRC Press, 2001.

[58] I.E. Telatar and D.N.C. Tse, "Capacity and mutual information of wideband multipath fading channels," *IEEE Trans. Inform. Theory*, vol. 46, no. 4, pp. 1384–1400, 2000.

[59] Z. Tian and G.B. Giannakis, "BER sensitivity to mis-timing in Ultra-Wideband communications," *IEEE Trans. Signal Processing*, to be published.

[60] Z. Tian and G.B. Giannakis, "Data-aided ML timing acquisition in Ultra-Wideband radios," in *Proc. Conf. Ultra-Wideband Systems and Technologies*, Reston, VA, 2003, pp. 142–146.

[61] Z. Tian, L. Yang, and G.B. Giannakis, "Symbol timing estimation in Ultra-Wideband communications," in *Proc. Asilomar Conf. Signals, Systems, and Computers*, Pacific Grove, CA, 2002, pp. 1924–1928.

[62] S. Tilak, N.B. Abu-Ghazaleh, and W. Heinzelman, "A taxonomy of wireless micro-sensor network models," *Mobile Computing Commun. Rev.*, vol. 6, no. 2, pp. 28–36, 2002.

[63] V. Tripathi, A. Mantravadi, and V.V. Veeravalli, "Channel acquisition for wideband CDMA signals," *IEEE J. Select. Areas Commun.*, vol. 18, no. 8, pp. 1483–1494, 2000.

[64] S. Verdú, "Wireless bandwidth in the making," *IEEE Commun. Mag.*, vol. 38, no. 7, pp. 53–58, 2000.

[65] S. Verdú, "Spectral efficiency in the wideband regime," *IEEE Trans. Inform. Theory*, vol. 48, no. 6, pp. 1319–1343, 2002.

[66] Z. Wang, "Multi-carrier ultra-wideband multiple-access with good resilience against multiuser interference," in *Proc. Conf. Info. Sciences and Systems*, Baltimore, MD, 2003.

[67] Z. Wang and G.B. Giannakis, "Wireless multicarrier communications: Where Fourier meets Shannon," *IEEE Signal Processing Mag.*, vol. 17, no. 3, pp. 29–48, 2000.

[68] Z. Wang and X. Yang, "Ultra wide-band communications with blind channel estimation based on first-order statistics," in *Proc. Int. Conf. Acoustics, Speech, and Signal Processing,* Montreal, Quebec, Canada, 2004, pp. 529–532.

[69] M.L. Welborn, "System considerations for Ultra-Wideband wireless networks," in *Proc. IEEE Radio Wireless Conf.*, Boston, MA, 2001, pp. 5–8.

[70] M.Z. Win, "On the power spectral density of digital pulse streams generated by m-ary cyclostationary sequences in the presence of stationary timing jitter," *IEEE Trans. Commun.*, vol. 46, no. 9, pp. 1135–1145, 1998.

[71] M.Z. Win, G. Chrisikos, and N.R. Sollenberger, "Performance of rake reception in dense multipath channels: implications of spreading bandwidth and selection diversity order," *IEEE J. Select. Areas Commun.*, vol. 18, no. 58, pp. 1516–1525, 2000.

[72] M.Z. Win and R.A. Scholtz, "Ultra wide bandwidth time-hopping spread-spectrum impulse radio for wireless multiple access communications," *IEEE Trans. Commun.*, vol. 48, no. 4, pp. 679–691, 2000.

[73] M.Z. Win and R.A. Scholtz, "Characterization of Ultra-Wide bandwidth wireless indoor channels: a communication-theoretic view," *IEEE J. Select. Areas Commun.*, vol. 20, no. 9, pp. 1613–1627, 2002.

[74] P. Withington, "Impulse radio overview," [Online]. Available: http://user.it.uu.se/~carle/Notes/UWB.pdf

[75] X. Wu, Z. Tian, T.N. Davidson, and G.B. Giannakis, "Optimal waveform design for UWB radios," *in Proc. Int. Conf. Acoustics, Speech, and Signal Processing*, Montreal, Canada, 2004, pp. 521–524.

[76] L. Yang and G.B. Giannakis, "Multi-stage block-spreading for impulse radio multiple access through ISI channels," *IEEE J. Select. Areas Commun.*, vol. 20, no. 9, pp. 1767–1777, 2002.

[77] L. Yang and G.B. Giannakis, "Digital-carrier multi-band user codes for baseband UWB multiple access," *J. Commun. Networks*, vol. 5, no. 4, pp. 374–385, 2003.

[78] L. Yang and G.B. Giannakis, "Analog space-time coding for multi-antenna Ultra-Wideband transmissions," *IEEE Trans. Commun.*, vol. 52, no. 3, pp. 507–517, 2004.

[79] L. Yang and G.B. Giannakis, "Blind UWB timing with a dirty template," in *Proc. Int. Conf. Acoustics, Speech, and Signal Processing*, Montreal, Quebec, Canada, 2004, pp. 509–512.

[80] L. Yang and G.B. Giannakis, "Cross-band flexible UWB multiple access for high-rate multi-piconet WPANs," in *Proc. Asilomar Conf. Signals, Systems, and Computers*, Pacific Grove, CA, 2004.

[81] L. Yang and G.B. Giannakis, "Optimal pilot waveform assisted modulation for Ultra-Wideband communications," *IEEE Trans. Wireless Commun.*, vol. 3, no. 4, pp. 1236–1249, 2004.

[82] L. Yang and G.B. Giannakis, "A general model and SINR analysis of low duty-cycle UWB access through multipath with NBI and Rake reception," *IEEE Trans. Wireless Commun.*, to be published.

[83] L. Yang, G.B. Giannakis, and A. Swami, "Noncoherent ultra-wideband radios," in *Proc. MILCOM Conf.*, Monterey, CA, 2004.

[84] H. Zhang and D.L. Goeckel, "Generalized transmitted-reference UWB systems," in *Proc. Conf. Ultra-Wideband Systems and Technologies*, Reston, VA, 2003, pp. 147–151.